CR-172004

FINITE ELEMENT SOLUTION TECHNIQUES FOR LARGE-SCALE PROBLEMS IN COMPUTATIONAL FLUID DYNAMICS

by

J. Liou [1]

and

T. E. Tezduyar [2]

Department of Mechanical Engineering
University of Houston
Houston, Tx 77004

---

(1) Graduate Research Assistant

(2) Assistant Professor

ABSTRACT

Element-by-element approximate factorization, implicit-explicit and adaptive implicit-explicit approximation procedures are presented for the finite–element formulations of large-scale fluid dynamics problems. The element-by-element approximation scheme totally eliminates the need for formation, storage and inversion of large global matrices. Implicit-explicit schemes, which are approximations to implicit schemes, substantially reduce the computational burden associated with large global matrices. In the adaptive implicit-explicit scheme, the implicit elements are selected dynamically based on element level stability and accuracy considerations. This scheme provides implicit refinement where it is needed.

The methods are applied to various problems governed by the convection-diffusion and incompressible Navier-Stokes equations. In all cases studied, the results obtained are indistinguishable from those obtained by the implicit formulations.

TABLE OF CONTENTS

LIST OF FIGURES

LIST OF FIGURES

FIGURE   PAGE

CHAPTER 1

INTRODUCTION

Significant improvements have been made in computer memory and speed in recent years. However, the existing computer power is still far behind the demands from scientists for large-scale fluid dynamics calculations. Implicit schemes, which are desirable for their stability and accuracy properties, lead to large global coefficient matrices which need to be formed, stored and inverted. Direct management of such matrices is very difficult for large-scale, geometrically complicated two-dimensional problems and is virtually impossible for large-scale three-dimensional problems. For example, a cubic domain with 30 nodal points along each side and with four unknowns at every node will produce some 108,000 equations with 7.8×10^8 entries in the global coefficient matrix. Even with the currently available supercomputers it is almost hopeless to try to handle directly such a large equation system.

To overcome the shortage of computer power, many researchers have developed algorithms for large-scale problems. In their application of domain decomposition methods, Glowinski, Dinh and Periaux [1] successfully coupled the incompressible viscous flow and incompressible potential flow models employed in different subdomains. A conjugate-gradient method, which is basically suitable for the symmetric and positive-definite systems, was employed to solve the variational problem. For the nonsymmetric and nonpositive-definite systems, one has to find an appropriate preconditioner for each problem; this needs much sophisticated work

[2-4]. A three-dimensional flow simulation with 128^3 nodal points was made by Rogallo [5] with the alternating-direction method. A new class of algorithms in numerical linear algebra which take advantage of the parallel computation capabilities of modern computers also provides hope [6].

In this report, we present element-by-element (EBE) approximate factorization, implicit-explicit (IMEX), and adaptive implicit-explicit (AIE) schemes for large-scale computations in fluid dynamics. Compared to implicit methods, these schemes possess, to a great extent, similar desirable stability and accuracy properties, yet result in substantial reduction in computer memory and CPU time demands.

The element-by-element approximate factorization is in some sense related to domain-decomposition [1,7] and alternating-direction (or operator-splitting) [8-11] schemes. These schemes, contrary to the EBE method, are based on global approximations. The EBE method was first proposed by Hughes, Levit and Winget [12,13] with applications to transient heat conduction, structural and solid mechanics problems. Preliminary application to fluid mechanics problems within the context of the compressible Euler equations were presented in Hughes, Levit, Winget and Tezduyar [14]. In this report, we present our EBE formulation for problems with nonsymmetric, nonpositive-definite spatial differential operators. Currently we focus on the convection-diffusion and the incompressible Navier-Stokes equations. In the EBE formulation, global coefficient matrices are approximated by sequential product of much simpler matrices which are based on the most natural unit in the finite-element method, the element-level matrix. Every calculation is done at the element level. The method keeps the versatility of the finite-element formulation in its easy adjustment to irregular meshes. Other advantages of the finite-element method such as easy implementation of the boundary conditions and the source terms are also retained in the

EBE formulation.

Our implicit-explicit approximation schemes for fluid dynamics problems are based on the work of Hughes and Liu [15,16] which was for solid mechanics and heat transfer applications. We consider problems governed by the convection-diffusion and the incompressible Navier-Stokes equations. In this approach, for the elements which are designated to be implicit, the element level matrices are kept as they are, whereas for the explicit elements the element level matrices are approximated by a diagonal matrix. The implicit element-explicit element decision is based on the local stability criterion.

In the adaptive implicit-explicit scheme the implicit element-explicit element decision is made dynamically. The stability and accuracy criteria applied to each element, based on the solution from the previous iteration or previous time step, determine whether an element needs to be implicit. In this approach we can adaptively have implicit refinement where it is needed for stability and accuracy. Compared to other adaptive schemes which are based on element redistribution or element subdividing [17], the AIE approach involves minimal bookkeeping and no geometric constraints; therefore the method is very easy to implement.

In Chapter 2, model problems are described and their spatial and temporal discretizations are given. In Chapter 3, the stability and accuracy analysis needed for the development of the IMEX and AIE schemes is performed. The EBE, IMEX, and AIE schemes are discussed in Chapters 4 and 5. Numerical results are presented in Chapter 6 and the conclusions are given in Chapter 7.

CHAPTER 2

MODEL PROBLEMS – SPATIAL AND TEMPORAL
DISCRETIZATIONS

We consider model problems governed by the convection-diffusion equation and the vorticity stream-function formulation of the two-dimensional incompressible Navier-Stokes equations. A formal statement of the problems and the corresponding spatial and temporal discretization for both cases are given below.

Convection-Diffusion Equation

Let Ω and Γ denote the computational domain and its boundary. Time-dependent convection-diffusion of an unknown scalar function Φ is governed by the following set of differential equations, boundary conditions, and initial condition:

$$\Phi_{,t} + u \cdot \nabla \Phi = \nabla \cdot (\kappa \nabla \Phi) + f, \qquad \text{on } \Omega \times] 0,T [\qquad (2.1)$$

$$\Phi (x , t) = g (x , t), \qquad \forall x \in \Gamma_g, t \in] 0,T [\qquad (2.2)$$

$$n \cdot \kappa \nabla \Phi (x , t) = h (x , t), \qquad \forall x \in \Gamma_h, t \in] 0,T [\qquad (2.3)$$

and

$$\Phi (x , 0) = \Phi_0(x), \qquad \text{on } \Omega \qquad (2.4)$$

where the velocity field $u = u (x)$ is given and κ is the conductivity matrix. The

source term is given as $f = f(x, t)$. The outward unit vector normal to the boundary Γ is denoted by n, whereas g, h and Φ_0 are prescribed functions. Γ_g and Γ_h are the mutually exclusive but complementary subsets of the boundary Γ with Dirichelet and Neumann boundary conditions respectively. That is,

$$\emptyset = \Gamma_g \cap \Gamma_h \qquad (2.5)$$

$$\Gamma = \Gamma_g \cup \Gamma_h \qquad (2.6)$$

Multiplying equation (2.1) by the weighting function $\tilde{w}$ and applying Green's theorem, we obtain the following weak form,

$$\int_\Omega \tilde{w} \, \Phi_{,t} \, d\Omega + \int_\Omega \tilde{w} \, u \cdot \nabla\Phi \, d\Omega + \int_\Omega \nabla\tilde{w} \cdot (\kappa \nabla\Phi) \, d\Omega$$

$$= \int_{\Gamma_h} \tilde{w} \, h \, d\Gamma + \int_\Omega \tilde{w} \, f \, d\Omega \qquad (2.7)$$

and

$$\int_\Omega \tilde{w} \, (\Phi - \Phi_0) \, d\Omega = 0 \qquad (2.8)$$

Finite-element spatial discretization of equations (2.7) and (2.8) leads to the following semi-discrete equations:

$$\tilde{M} \, \dot{\Phi} + \tilde{C} \, \Phi = \tilde{F} \qquad (2.9)$$

$$\Phi(0) = \Phi_0, \qquad (2.10)$$

5

where $\widetilde{M}$, $\widetilde{C}$ and $\widetilde{F}$ are the "mass" matrix, "stiffness" matrix, and the generalized "force" vector, respectively; Φ and $\dot{\Phi}$ represent the dependent variable and its temporal derivative at the nodes. The information regarding the initial condition is contained in vector Φ_0.

Burger's equation, given below, can be treated as a special case of the convection-diffusion equation,

$$\Phi_{,t} + \Phi\,\Phi_{,x} = 0 \qquad \forall\, x \in \,]\,0,L\,[,\;\; t \in \,]\,0,T\,[\qquad\qquad (2.11)$$

This simple nonlinear hyperbolic equation is used to study the numerical performance related to shock formulation and entropy condition. A finite-element discretization of this equation leads to the following semi-discrete nonlinear equation system,

$$\widetilde{M}\,\dot{\Phi} + N\,(\Phi) = \widetilde{F}, \qquad\qquad (2.12)$$

where $N\,(\Phi)$ is a nonlinear function of Φ.

Vorticity Stream-Function Form of the Two-Dimensional Incompressible Navier-Stokes Equations

The incompressibility condition and the nonlinear convection term constitute some of the major difficulties for the numerical methods associated with the Navier-Stokes equations. By employing a vorticity stream-function formulation, one can easily handle the incompressibility condition. However, the extension of the numerical algorithm to three-dimensional problems is rather cumbersome and the treatment of the boundary conditions on no-slip surfaces and at out-flow boundaries is

complicated (see, e.g., [18]). The field equations consist of a time-dependent transport equation for the unknown vorticity function ω and an equation which relates the unknown stream function Ψ to vorticity. They are given as follows:

$$\omega_{,t} + \mathbf{u} \cdot \nabla \omega = \nu\, \nabla^2 \omega \qquad \text{on } \Omega \times]\,0,T\,[\qquad (2.13)$$

and

$$\nabla^2 \Psi = -\,\omega, \qquad \text{on } \Omega \qquad (2.14)$$

where ν is the kinematic viscosity. The velocity field $\mathbf{u}$, which is now an unknown, is related to the stream function by the following equations:

$$u_1 = \partial \Psi / \partial x_2 \qquad (2.15)$$

and

$$u_2 = -\,\partial \Psi / \partial x_1 \qquad (2.16)$$

Note that equations (2.15) and (2.16) lead to a zero-divergence condition,

$$\nabla \cdot \mathbf{u} = \partial^2 \Psi / \partial x_2\, \partial x_1 - \partial^2 \Psi / \partial x_1\, \partial x_2 = 0 \qquad (2.17)$$

In other words, the incompressibility condition on $\mathbf{u}$ is assured by the definition of Ψ.

The boundary conditions for ω and Ψ are given below:

$$\omega\,(\,\mathbf{x},t\,) = \tilde{g}\,(\,\mathbf{x},t\,), \qquad \forall\, \mathbf{x} \in \Gamma_{\tilde{g}}, \quad t \in]\,0,T\,[\qquad (2.18)$$

$$\nu\,\mathbf{n} \cdot \nabla \omega\,(\,\mathbf{x},t\,) = \tilde{h}\,(\,\mathbf{x},t\,), \qquad \forall\, \mathbf{x} \in \Gamma_{\tilde{h}}, \quad t \in]\,0,T\,[\qquad (2.19)$$

$$\Psi\,(\,\mathbf{x},t\,) = g\,(\,\mathbf{x},t\,), \qquad \forall\, \mathbf{x} \in \Gamma_g, \quad t \in]\,0,T\,[\qquad (2.20)$$

and

$$\mathbf{n} \cdot \nabla \Psi (\mathbf{x}, t) = h (\mathbf{x}, t), \qquad \forall \mathbf{x} \in \Gamma_h, \quad t \in]0, T[\qquad (2.21)$$

where $\Gamma_{\tilde{g}}$ and $\Gamma_{\tilde{h}}$ are the mutually exclusive but complementary subsets of the boundary Γ with Dirichelet and Neumann boundary conditions for ω, whereas Γ_g and Γ_h are similar boundary subsets for Ψ; that is

$$\varnothing = \Gamma_{\tilde{g}} \cap \Gamma_{\tilde{h}} \qquad (2.22)$$

$$\Gamma = \Gamma_{\tilde{g}} \cup \Gamma_{\tilde{h}} \qquad (2.23)$$

and

$$\varnothing = \Gamma_g \cap \Gamma_h \qquad (2.24)$$

$$\Gamma = \Gamma_g \cup \Gamma_h \qquad (2.25)$$

The difficulty associated with the lack of boundary conditions for the vorticity and its normal derivative on no-slip surfaces can be handled by a discrete Green's formula approach which is described in Tezduyar, Glowinski, and Glaisner [19].

The initial condition for the vorticity is given as

$$\omega (\mathbf{x}, 0) = \omega_0 \qquad \text{on } \Omega \qquad (2.26)$$

Multiplying (2.13) and (2.14) by weighting functions $\tilde{w}$ and w respectively, the following weak forms can be obtained via the Green's theorem:

$$\int_\Omega \tilde{w} \, \omega_{,t} \, d\Omega + \int_\Omega \tilde{w} \, \mathbf{u} \cdot \nabla \omega \, d\Omega + \int_\Omega \nabla \tilde{w} \cdot v \, \nabla \omega \, d\Omega$$

$$= \int_{\Gamma_{\tilde{h}}} \tilde{w} \, \tilde{h} \, d\Gamma \qquad (2.27)$$

and

$$\int_\Omega w\,\omega\,d\Omega \; + \; \int_\Omega \nabla\omega\cdot\nabla\Psi\,d\Omega \; = \; \int_{\Gamma_h} w\,h\,d\Gamma \qquad\qquad (2.28)$$

Finite-element spatial discretization of equations (2.27) and (2.28) leads to the following set of equations:

$$\tilde{M}\,\dot{\omega} + \tilde{K}\,\omega = \tilde{F}, \qquad\qquad (2.29)$$

$$\omega\,(\,0\,) = \omega_0, \qquad\qquad (2.30)$$
and

$$-\,M\,\omega + K\,\Psi = F, \qquad\qquad (2.31)$$

where $\tilde{M}$, $\tilde{K}$, $\tilde{F}$, M, K, and F are the matrices and vectors resulting from the spatial discretization; ω, $\dot{\omega}$, and Ψ represent the vorticity, its temporal derivative and the stream function at the nodes. The initial condition for ω is represented by ω_0.

Spatial Discretization

Due to the existence of nonsymmetric spatial operators (convection terms) in our model problems, the "best approximation" property of the Galerkin finite element formulations [20] is lost, and therefore spurious oscillations can be encountered in convection-dominated problems. Streamline-Upwind/Petrov-Galerkin (SUPG) formulations are employed for the spatial discretization of our model problems. These formulations are well-known for their robust and accurate performance for problems with nonsymmetric spatial operators. Several papers can be found in scientific

literature on this type of schemes (see, e.g., [21, 22]). For the purpose of this thesis, we briefly describe the SUPG scheme employed in terms of the weighting function basis $\tilde{N}_a$; this description is given by

$$\tilde{N}_a = N_a + C_{2\tau} h /2 \, s \cdot \nabla N_a \qquad (2.32)$$

or

$$\tilde{N}_a = N_a + \tau \, u \cdot \nabla N_a, \qquad (2.33)$$

where the subscript "a" refers to an element node, N_a is the solution function basis, h is the "element length" in the direction of u, and s is the unit vector in u direction. The "algorithmic Courant number" $C_{2\tau}$ and the "algorithmic time constant" τ are related by the following expression,

$$C_{2\tau} = \| u \| \, 2 \tau / h. \qquad (2.34)$$

Temporal Discretization

Consider the following general semi-discrete equation system related to our model problems:

$$M \, a + N \, (v) = F \qquad (2.35)$$

$$v \, (\, 0 \,) = v_0. \qquad (2.36)$$

where the vector a is the temporal derivative of the vector v. $N \, (v)$ is a vector-valued function of v which we will, in general, assume to be nonlinear.

The tangent " stiffness matrix" K is defined as

$$K = \partial N (v) / \partial v \qquad\qquad (2.37)$$

A predictor/multi-corrector transient integration algorithm [23] is employed to solve equations (2.35) and (2.36). Let a subscript denote the time step and a superscript denote the iteration step. The algorithm can be summarized as follows:

1. given v_0, find a_0 from

$$M\ a_0 + N\ (v_0) = F_0 \qquad\qquad (2.38)$$

$n \rightarrow n+1$

2. predictor stage

$$v_{n+1}^0 = v_n + (\ 1-\alpha\ )\ \Delta t\ a_n \qquad\qquad (2.39)$$

$$a_{n+1}^0 = 0 \qquad\qquad (2.40)$$

$i \rightarrow i+1$

3. corrector stage

$$R_{n+1}^i = F_{n+1} - M\ a_{n+1}^i - N\ (v_{n+1}^i) \qquad\qquad (2.41)$$

$$M^* \Delta a_{n+1}^i = R_{n+1}^i \qquad\qquad (2.42)$$

$$a_{n+1}^{i+1} = a_{n+1}^i + \Delta a_{n+1}^i \qquad\qquad (2.43)$$

and

$$v_{n+1}^{i+1} = v_{n+1}^i + \alpha\ \Delta t \Delta a_{n+1}^i, \qquad\qquad (2.44)$$

where $\alpha \in [\ 0,1]$ is a parameter which controls the stability and accuracy.

Convergence is checked by inspecting the norm of $R_{n+1}{}^i$ and $\Delta a_{n+1}{}^i$.

Remark:

1. A consistent derivation for M^* gives the following expression,

$$M^* = M + \alpha \, \Delta t \, K \tag{2.45}$$

If left as it is, this expression for M^* leads to an <u>implicit</u> formulation which requires only one correction for linear systems. However, for nonlinear systems, one needs to have as many corrections as the convergence criterion dictates.

2. A choice of

$$M^* = M_L \tag{2.46}$$

where M_L is a lumped version of matrix M, leads to an <u>explicit</u> formulation. Explicit formulations in general are less stable, less accurate, but also less costly (less memory and less CPU time) compared to implicit schemes. The conditional stability of these methods are usually expressed in terms of a limit on the element Courant number. The element Courant number $C_{\Delta t}$ is defined as

$$C_{\Delta t} = \| u \| \, \Delta t / h \tag{2.47}$$

3. In the SUPG formulation, the choice of

$$\tau = \alpha \, \Delta t \tag{2.48}$$

leads to a symmetric positive-definite M^* for pure convection problems.

12

<u>Proof</u>:

A general convection equation is given as

$$\Phi_{,t} + u \cdot \nabla \Phi = f \qquad (2.49)$$

The following semi-discrete (spatially continuous) formulation can be obtained from equation (2.49),

$$(\Phi_{n+1} - \Phi_n) / \Delta t + u \cdot \nabla ((1-\alpha) \Phi_n + \alpha \Phi_{n+1})$$

$$= (1-\alpha) f_n + \alpha f_{n+1} \qquad (2.50)$$

For the weak form of equation (2.50), we employ a weighting function $\tilde{w}$ which is given as

$$\tilde{w} = w + \tau u \cdot \nabla w, \qquad (2.51)$$

where w and Φ come from the same space. Note that for this pure convection system, a Dirichlet type boundary condition for Φ is required on the part of the boundary where the information comes from outside the domain, and w has to satisfy the homogeneous form of the same boundary condition. That is,

$$\Phi(x) = g(x) \qquad \forall x \in \{ x \mid x \in \Gamma, n(x) \cdot u(x) < 0 \} \qquad (2.52)$$

and

$$w(x) = 0 \qquad \forall x \in \{ x \mid x \in \Gamma, n(x) \cdot u(x) < 0 \} \qquad (2.53)$$

The weak form of equation (2.50) with the weighting function of equation

(2.51) can be written as

$$(w, \Phi_{n+1}) + \alpha \, \Delta t \, (w, u \cdot \nabla \Phi_{n+1}) + \alpha \, \Delta t \, (u \cdot \nabla w, \Phi_{n+1}) +$$

$$(\alpha \, \Delta t)^2 \, (u \cdot \nabla w, \; u \cdot \nabla \Phi_{n+1}) \;\; = \;\; \text{right hand side} \qquad (2.54)$$

where the bilinear form $(\bullet, \bullet)$ is defined as

$$(w, \Phi) \;\; = \;\; \int_{\Omega} w \, \Phi \, d\Omega \qquad\qquad (2.55)$$

Note that only the left hand side of equation (2.54) corresponds to M^*. Rewriting equation (2.54), we get

$$(w + \alpha \, \Delta t \, u \cdot \nabla w, \; \Phi_{n+1} + \alpha \, \Delta t \, u \cdot \nabla \Phi_{n+1}) \;\; = \;\; \text{righe hand side} \qquad (2.56)$$

We need to show that the left hand side of equation (2.56) has a symmetric positive-definite form. It is obvious that this bilinear form is symmetric and that

$$(w + \alpha \, \Delta t \, u \cdot \nabla w, \; w + \alpha \, \Delta t \, u \cdot \nabla w) \;\; \geq \;\; 0 \qquad\qquad (2.57)$$

We have to show that if

$$(1 / \alpha \, \Delta t) \, w + u \cdot \nabla w \;\; = \;\; 0, \qquad\qquad (2.58)$$

then

$$w = 0 \qquad\qquad (2.59)$$

14

Note that equation (2.58) is nothing more than a linear, steady-state, convection-reactiontype equation for w. Since $(1/\alpha \Delta t)$ is always positive, the reaction is a consumption on w. If the value of w at any point can be traced back to a boundary point, because of equation (2.53), $w = 0$; if not, $w = 0$ because of consumption. This completes our proof, based partly on physical reasoning, that M^* is symmetric positive-definite.

CHAPTER 3

STABILITY AND ACCURACY ANALYSIS

In convection-dominated problems, Galerkin formulation, just like the classical central-difference schemes, generates numerical oscillations especially in the presence of sharp layers. To minimize these oscillations, one can refine the grid at the oscillation zones, but then must pay for increased memory and CPU costs. Another option is the classical upwind scheme which leads to forward- or backward-difference treatment of the convection terms depending on the direction of the convection velocity. With this option, while the wiggles are minimized, usually an excessive amount of artificial diffusion is introduced into the numerical simulation. To explain this, let us consider a simple one-dimensional convection problem,

$$\Phi_{,t} + u\,\Phi_{,x} = 0, \qquad\qquad (3.1)$$

where $u > 0$ is the convection velocity. For the node numbered i at time step $n+1$, the upwind scheme leads to the following fully discrete equation,

$$(1/\Delta t)\,(\Phi_i^{n+1} - \Phi_i^n) + u\,(1/h)\,(\Phi_i^{n+1} - \Phi_{i-1}^{n+1}) = 0, \qquad\qquad (3.2)$$

in which Δt is the time integration step and h is the spatial discretization step. It is clear that equation (3.2) can be rewritten as

$$(1/\Delta t) \, (\Phi_i^{n+1} - \Phi_i^n) + u \, (1/2h) \, (\Phi_{i+1}^{n+1} - \Phi_{i-1}^{n+1})$$

$$- (u \, h \, / \, 2) \, (1/h^2) \, (\Phi_{i+1}^{n+1} + \Phi_{i-1}^{n+1} - 2\Phi_i^{n+1}) = 0 \qquad (3.3)$$

Returning to the continuous counterpart of equation (3.3), we obtain

$$\Phi_{,t} + u \, \Phi_{,x} - (u \, h \, / \, 2) \, \Phi_{,xx} = 0 \qquad (3.4)$$

It can be observed that, compared to equation (3.1), an artificial diffusion term with coefficient value of (uh / 2) has been introduced into the continuous equation by the upwind scheme. For high convection velocities and large elements, the artificial diffusion becomes significant. This results in simulations which depart substantially from the real physical phenomenon.

Streamline-Upwind/Petrov-Galerkin formulations [21,22] keep the numerical oscillations and the level of artificial diffusion to a minimum. Weighting functions leading to the SUPG formulations are described by equations (2.1)-(2.3). Tezduyar and Ganjoo [21] have investigated the various choices of the $C_{2\tau}$ term in the SUPG formulations by a phase accuracy and amplitude analysis for a one-dimensional transient pure convection equation (3.1). These choices of the $C_{2\tau}$ term are

$$C_{2\tau} = 1 \qquad \text{(choice 1)} \qquad (3.5)$$

$$C_{2\tau} = C_{\Delta t} \qquad \text{(choice 2)} \qquad (3.6)$$

$$C_{2\tau} = 2/\sqrt{15} + (1 - 2/\sqrt{15}) \, C_{\Delta t} \qquad \text{(choice 3)} \qquad (3.7)$$

17

In [21], the exact solution of equation (3.1) is assumed to be of the form,

$$\Phi(x,t) = e^{-(\xi+i\omega)t} e^{-ikx} \qquad (3.8)$$

and the finite-element solution is of the form,

$$\Phi(x_i,t_n) = e^{-(\tilde{\xi}+i\tilde{\omega})n\Delta t} e^{-ikx_i}, \qquad (3.9)$$

where ξ and $\tilde{\xi}$ are the exact and approximate damping rates; ω and $\tilde{\omega}$ represent the exact and approximate frequencies. The wave number is denoted by k ($k = 2\pi/\lambda$, λ is the wave length). The significant quantities in this analysis are the algorithmic damping ratio (ADR $= \tilde{\xi}/\tilde{\omega}$) and the frequency ratio (FR $= \tilde{\omega}/\omega$). A good scheme should have an ADR approaching zero and a FR approaching unity. From the rates these quantities approach these limits, one can infer the order of accuracy of the algorithm.

Let h denote the element length; a dimensionless wave number is defined as

$$q = k\,h \qquad (3.10)$$

This is a measure of the spatial refinement of the numerical method. Figures 3.1-3.3, adopted from [21], show the ADR and FR values versus q for a set of element Courant numbers and various choices of $C_{2\tau}$. The order of accuracy can be revealed from the ADR and FR curves. A scheme is first-order accurate if either of the curves has a finite slope as q approaches zero. It is at least second-order accurate if both curves have zero slopes as q approaches zero. It can be seen that all implicit schemes have at least second-order accuracy. In fact, choice 3 leads to a fourth-order accurate scheme [24] as $C_{\Delta t}$ approaches zero. For explicit one-pass schemes,
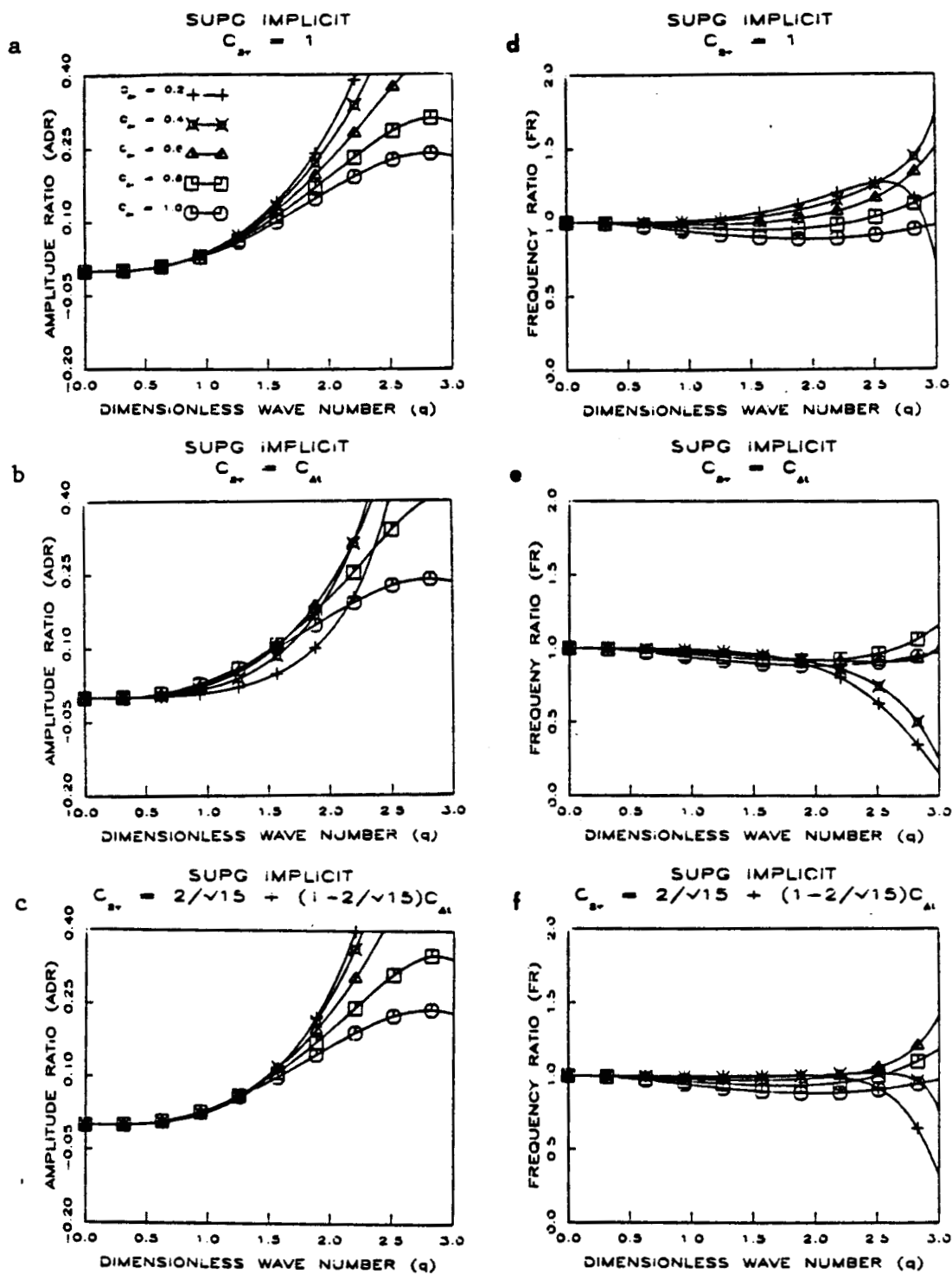
18

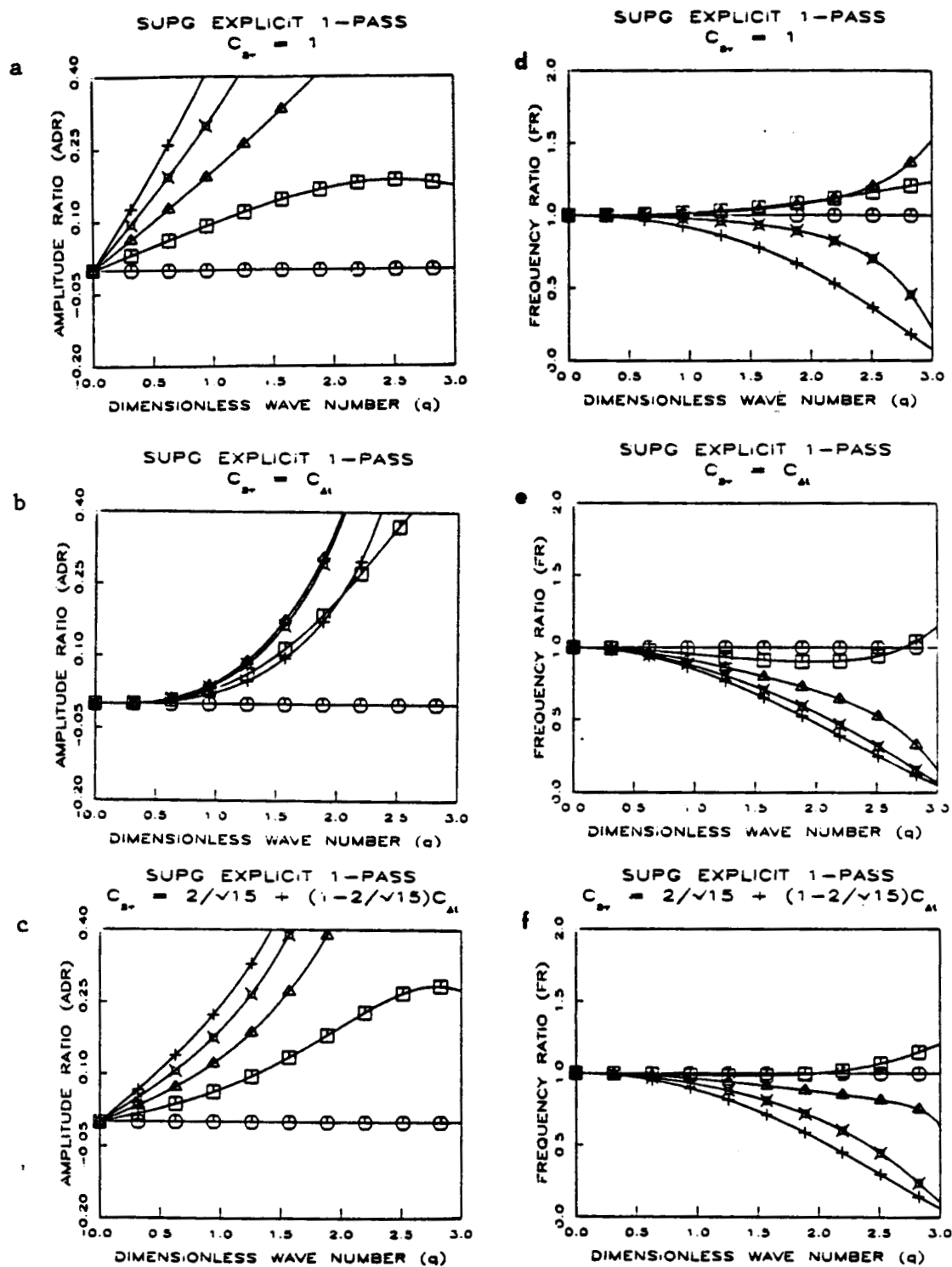Fig. 3.1 Stability and accuracy characteristics for the implicit SUPG formulation.

19

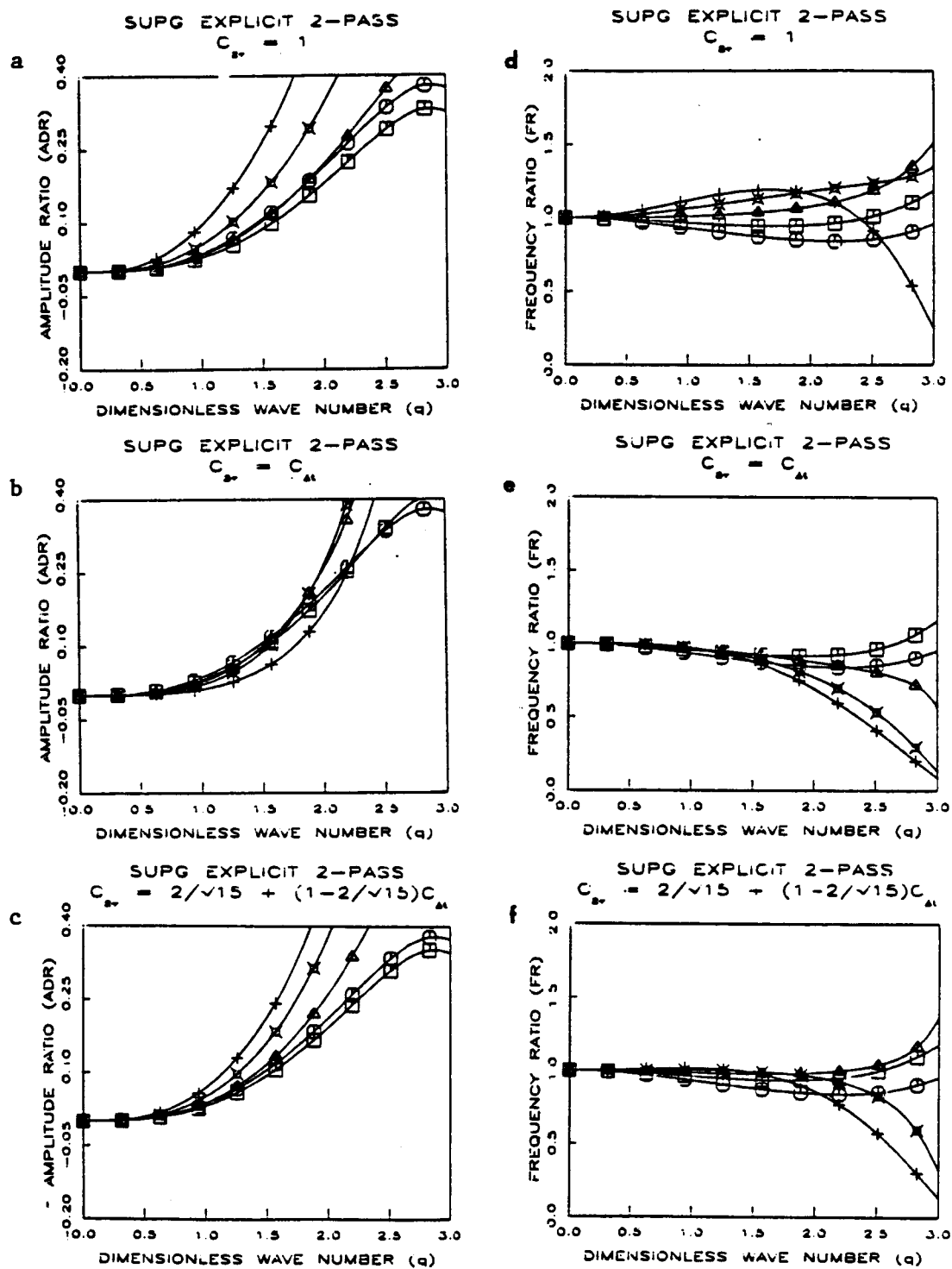Fig. 3.2 Stability and accuracy characteristics for the explicit one-pass SUPG formulation.

20

Fig. 3.3 Stability and accuracy characteristics for the explicit two-pass SUPG formulation.

21

choice 2 gives second-order accuracy. All explicit two-pass schemes are second-order accurate.

Based on a single degree of freedom model analysis performed by Tezduyar and Hughes [25] for the one-dimensional convection equation, we obtain the following stability conditions:

1. Implicit scheme:

   All choices of $C_{2\tau}$ are unconditionally stable for $\alpha \geq 1/2$ and $r \leq 1/4$ where r is a parameter which depends on the numerical integration technique used for the time dependent terms. Typical values are $r = 0$ for lumped mass, $r = 1/6$ for consistent mass and $r = 1/4$ for PG (pade) mass (see [21]).

2. Explicit one-pass schemes:

   All choices of $C_{2\tau}$ are conditionally stable; the stability criterion yields

$$C_{\Delta t} < \frac{2\, C_{2\tau}}{2 - v\, (1 - C_{2\tau})} \tag{3.11}$$

   where $v = 1 - \cos q$. Note that, for Galerkin schemes ($C_{2\tau} = 0$), the method is unconditionally unstable. It can be shown that for all choices of $C_{2\tau}$ the stability limit is

$$C_{\Delta t} < 1 \tag{3.12}$$

3. Explicit two-pass schemes:

   The following inequality must be satisfied for stability:

$$2 \left(A_1 B_1 - A_2 B_2 \right) + \left(A_1{}^2 + A_2{}^2 \right) \left(B_1{}^2 + B_2{}^2 \right) < 0, \tag{3.13}$$

where

$$A_1 = C_{\Delta t} \, C_{2\tau} \, v \tag{3.14}$$

$$A_2 = C_{\Delta t} \, w \tag{3.15}$$

$$B_1 = \alpha \, C_{\Delta t} \, C_{2\tau} \, v - 1 - 2 \, r \, v \tag{3.16}$$

and

$$B_2 = \alpha \, C_{\Delta t} \, w - C_{2\tau} \, w/2, \tag{3.17}$$

in which $w = \sin q$. The worst case occurs for $q = \pi$ (which leads to $v = 2$ and $w = 0$); then equation (3.13) implies

$$4 \, C_{\Delta t} \, C_{2\tau} \left(2 \, \alpha \, C_{\Delta t} \, C_{2\tau} - 1 - 4r \right) \times$$

$$\{ \, 2 \, \alpha \, [\, C_{\Delta t} \, C_{2\tau} - (1 + 4r)/4\alpha]^2 + 1 - (1+4r)^2/8\alpha \, \} < 0 \tag{3.18}$$

It is obvious that under the choices of $\alpha \geq 1/2$ and $r \leq 1/4$,

$$1 - (1+4r)^2/8\alpha \geq 0, \tag{3.19}$$

then equation (3.18) leads to the following stability condition,

$$C_{\Delta t} \, C_{2\tau} < \frac{1 + 4 \, r}{2 \, \alpha} \tag{3.20}$$

For various choices of $C_{2\tau}$, the stability limits can be expressed as follows:

23

$$\text{choice 1:} \qquad C_{\Delta t} < \frac{1 + 4r}{2\alpha} \qquad\qquad (3.21)$$

$$\text{choice 2:} \qquad C_{\Delta t} < \left(\frac{1 + 4r}{2\alpha}\right)^{1/2} \qquad\qquad (3.22)$$

$$\text{choice 3:} \qquad C_{\Delta t} < \frac{-2/\sqrt{15} + \sqrt{4/15 + 4(1 - 2/\sqrt{15})(1 + 4r/2\alpha)}}{2(1 - 2/\sqrt{15})} \qquad\qquad (3.23)$$

Similar analysis has been done in one-dimensional diffusion equation for the Galerkin finite-element formulation. The conditional stability of the explicit schemes are expressed in terms of a limit on the diffusion Courant number. The diffusion Courant number C_κ is defined as

$$C_\kappa = 2\,\kappa\,\Delta t\,/\,h^2, \qquad\qquad (3.24)$$

where κ is the diffusion coefficient. The stability and accuracy properties can be summarized as follows:

1. Implicit scheme:

    a) Unconditional stability is assured for $\alpha \geq 1/2$ and $r \leq 1/4$.

    b) The algorithm is second-order accurate. It becomes fourth-order accurate with the choice of $r = 1/12$.

2. Explicit one-pass scheme:

   a) It is conditionally stable. The stability criterion is

   $$C_\kappa \leq 1 \tag{3.25}$$

   b) The algorithm is first-order accurate.

3. Explicit two-pass scheme:

   a) It is conditionally stable . The stability criterion is

   $$C_\kappa \leq \frac{1+4\,r}{2\,\alpha} \tag{3.26}$$

   b) The accuracy is of the same order as the implicit scheme.

CHAPTER 4

ELEMENT-BY-ELEMENT (EBE) APPROXIMATE
FACTORIZATION

The equation system of (2.42) can be rewritten as follows,

$$\mathbf{A} \ \mathbf{x} = \mathbf{b}, \tag{4.1}$$

where $\mathbf{x}$ is the increment vector $\Delta\mathbf{a}$, $\mathbf{b}$ is the residual vector $\mathbf{R}$, and $\mathbf{A}$ is the coefficient matrix $\mathbf{M}^*$.

A parabolic regularization of equation (4.1) can be expressed as

$$\mathbf{W} \ d\mathbf{y} \ / \ d\theta + \mathbf{A} \ \mathbf{y} = \mathbf{b}, \tag{4.2}$$

where θ is a dimensionless "pseudo-time" and

$$\mathbf{y} \ (\ 0 \ ) = 0 \tag{4.3}$$

We assume that

$$\mathbf{x} = \lim_{\theta \to \infty} \ \mathbf{y} \ (\ \theta \ ) \tag{4.4}$$

The choice of $\mathbf{W}$ depends on the properties of $\mathbf{A}$. For a symmetric positive-definite $\mathbf{A}$, Hughes, Levit and Winget [12,13] proposed $\mathbf{W}$ to be the

diagonal part of A,

$$W = \text{diag } A \tag{4.5}$$

This was found to be effective for all problems studied in [12,13]. Alternately W can be chosen to be the lumped mass matrix mentioned in Chapter 2. That is,

$$W = M_L \tag{4.6}$$

This choice was proposed by Hughes, Winget, Levit and Tezduyar [14].

We employ an unconditionally stable pseudo-time stepping algorithm given below:

$$(W + \alpha \, \Delta\theta \, A) \, \Delta y_m = \Delta\theta \, r_m \tag{4.7}$$

$$r_m = b - A \, y_m \tag{4.8}$$

and

$$y_{m+1} = y_m + \Delta y_m, \tag{4.9}$$

in which $\alpha \in [1/2, 1]$. The scheme is backward-Euler with $\alpha = 1$, and Crank-Nicolson with $\alpha = 0.5$. Equation (4.7) can also be written as

$$\Delta y_m = D \, (I + \alpha \, DAD)^{-1} \, D \, r_m, \tag{4.10}$$

where I is the identity matrix and

$$D = (W^{-1} \, \Delta\theta)^{1/2} \tag{4.11}$$

Note that equation (4.11) requires W to be positive-definite. While the choice of equation (4.5) does not guarantee this when M* is not positive-definite, the alternate

27

choice of equation (4.6) does. One also needs to note that for problems in fluid mechanics, M^* in general is not symmetric, positive-definite; however, as mentioned in Chapter 2, the choice of equation (2.50) assures that it is.

Since we are interested in the steady-state solution of equation (4.2), usually the backward-Euler scheme is adopted to avoid undamped and oscillating solutions as the condition number of the problem deteriorates or as large pseudo-time steps are chosen [26].

Rewriting equation (4.10) with the choice of $\alpha = 1$, we obtain

$$\Delta y_m = D (I + DAD)^{-1} D r_m \qquad (4.12)$$

The EBE approximate factorization is based on the following expressions:

1. one-pass EBE approximation:

$$(I + DAD) \approx \prod_{e=1}^{nel} (I + DA^e D), \qquad (4.13)$$

in which nel is the total number of elements in the domain, and A^e is the contribution of eth element (or subdomain) to A. Clearly, this approximation depends on the element ordering.

2. two-pass EBE approximation:

$$(I + DAD) \approx \prod_{e=1}^{nel} (I + 1/2\ DA^e D) \prod_{e=nel}^{1} (I + 1/2\ DA^e D) \qquad (4.14)$$

It should be noted that the approximation of the one-pass EBE deteriorates as a large $\Delta\theta$ is taken to assure a fast steady-state solution of equation (4.2). The two-pass EBE approximation has a better performance in this situation.

We update y_{m+1} according to the following formula,

$$y_{m+1} = y_m + s\,\Delta y_m, \tag{4.15}$$

where s is a search parameter obtained by minimizing $\| r_{m+1} \|^2$ with respect to s,

$$s = (A\,\Delta y_m){\cdot}r_m\,/\,\| A\,\Delta y_m \|^2 \tag{4.16}$$

Remark:

1. The need for the formation and storage of the global matrix A has been eliminated. There is no need to store the element level matrices A^e's; however, if desired, instead of recomputing for each EBE iteration, the element level matrices can be stored. Even then, the storage requirement is far less than that of a global matrix. For instance, in a cubic grid with N nodes at each side and one unknown at each node, $2N^5$ entries must be stored in the global matrix for the implicit calculation. EBE needs only 64 entries in each element matrix. Even if all element level matrices are stored, the total number of entries is only $64N^3$.

2. The EBE approximate factorization procedure is parallelizable. This aspect makes EBE favorable especially since parallel computations are expected to play a more and more important role in computational fluid dynamics.

3. It must be well understood that if the EBE procedure converges, it converges to the solution of equation (4.1), which is the equation system of the implicit method.

CHAPTER 5

IMPLICIT-EXPLICIT APPROXIMATION SCHEMES

In solving partial differential equations via finite-element method, since the solution may vary significantly in the domain, a nonuniform mesh is usually employed for stable, accurate, and efficient solution procedures. A finite element analyst can vary the element sizes in his/her nonuniform mesh anyway he / she pleases but usually according to some criteria based on past experience, physical intuition, and mathematical insight. Implicit schemes, though stable and accurate, may cost too much (CPU time and storage) to compute. To guarantee stable solutions for explicit schemes, one has to limit the time discretization step size based on the smallest element size in the entire domain. This may place a rather prohibitive constraint on the explicit integration scheme. The implicit-explicit approximation schemes provide an effective way to overcome these drawbacks. The basic idea associated with the implicit-explicit schemes can be well demonstrated by the following simple one-dimensional initial /boundary-value problem:

$$\Phi_{,t} + u\,\Phi_{,x} - \kappa\,\Phi_{,xx} = 0, \quad \forall\, x \in\,]\,0,1\,[\,,\, t \in [\,0,T\,] \qquad (5.1)$$

$$\Phi\,(\,0,t\,) = 1, \qquad\qquad \forall\, t \in [\,0,T\,] \qquad\qquad (5.2)$$

$$\Phi\,(\,1,t\,) = 0, \qquad\qquad \forall\, t \in [\,0,T\,] \qquad\qquad (5.3)$$

and

$$\Phi\,(\,x,0\,) = 0. \qquad\qquad \forall\, x \in\,]\,0,1\,[\qquad\qquad (5.4)$$

The steady-state analytical solution to equation (5.1) is

$$\Phi = \frac{e^{ux/\kappa} - e^{u/\kappa}}{1 - e^{u/\kappa}} \tag{5.5}$$

For sufficiently large u/κ, the solution is essentially unity in the interior of the domain, decaying through a boundary layer near $x = 1$ to assume the boundary value of $\Phi = 0$. In our computation, a finer mesh is employed in the right region of the domain as shown in Figure 5.1(a). A constant time step size is chosen such that the element Courant number is 0.7 in the left and 1.4 in the right regions. Figure 5.1(b) shows the solution obtained by the implicit scheme. Figure 5.1(c) shows the unstable solution obtained by the explicit one-pass scheme; this is due to the high Courant number in the right region. In the implicit-explicit scheme, we treat the elements in the right region implicitly and the ones in the left region explicitly. The solution is stable and accurate as shown in Figure 5.1(d).

Let $\mathcal{E}$ be the set of all elements, $e = 1,2,...,nel$. The assembly of the global matrix M^* can be expressed as follows,

$$M^* = \underset{e \in \mathcal{E}}{\textbf{A}} \, (m^*)^e, \tag{5.6}$$

where $\textbf{A}$ is the assembly operator.

Let $\mathcal{E}_I$ and $\mathcal{E}_E$ be the subsets of $\mathcal{E}$ corresponding to "implicit elements" and "explicit elements" respectively, such that

$$\mathcal{E} = \mathcal{E}_I \cup \mathcal{E}_E \tag{5.7}$$

and

$$\varnothing = \mathcal{E}_I \cap \mathcal{E}_E \tag{5.8}$$

31

a $x = 0.$ $x = 1.$

$$h_{Left} = 2\, h_{Right}$$

b

c

d
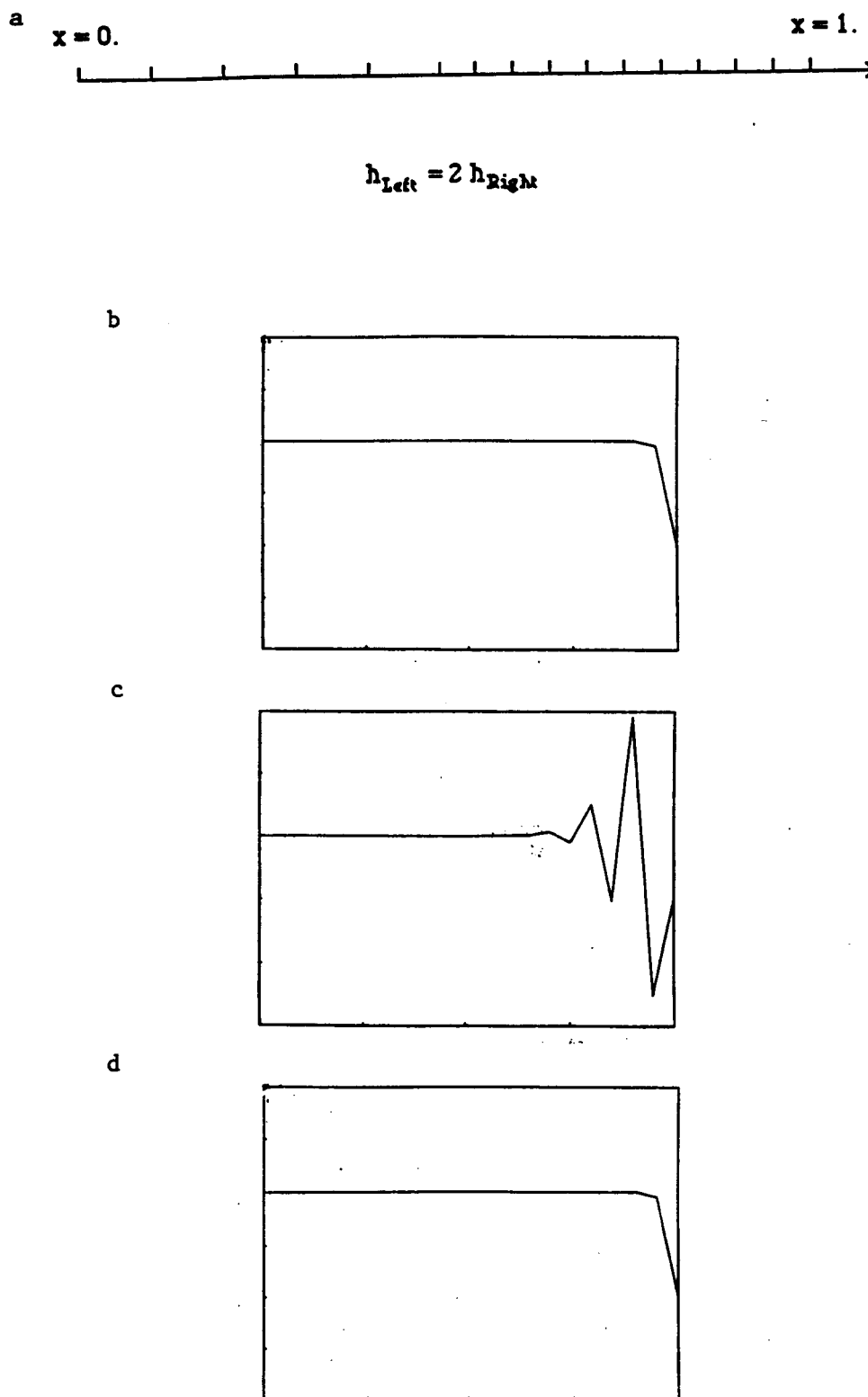
Fig. 5.1 One-dimensional boundary layer problem: (a) Finite element mesh.
Solutions by various schemes: (b) Implicit scheme. (c) Explicit one-pass scheme.
(d) Implicit-explicit one-pass scheme.

Rewriting equation (5.6), we get

$$M^* = \mathop{A}_{e \in \mathcal{E}_I} (m^*)^e + \mathop{A}_{e \in \mathcal{E}_E} (m^*)^e \qquad (5.9)$$

Implicit-explicit approximation [15,16] is based on the replacement of $(m^*)^e$ by the element level lumped mass matrix $(m)^e_L$,

$$M^* = \mathop{A}_{e \in \mathcal{E}_I} (m^*)^e + \mathop{A}_{e \in \mathcal{E}_E} (m)^e_L \qquad (5.10)$$

Let M^I and K^I denote respectively the mass matrix and stiffness matrix obtained by assembling the implicit elements and M^E denote the diagonal mass matrix from the explicit elements ($\alpha \Delta t\ K^E$ is neglected). An equivalent form of equation (5.10) can be expressed as

$$M^* = M^E + M^I + \alpha \Delta t\ K^I \qquad (5.11)$$

Many finite element simulations involve movement of fronts in the computational domain. The unknown variable can be the temperature in the heat equation, the vorticity in the Navier-Stokes equations, or the oil concentration in the enhanced oil recovery processes. Due to the presence of the convection operator and sharp layers in the solution, the solution is prone to instability and inaccuracy around the moving fronts. In such cases implicit-explicit schemes can be employed by concentrating the implicit elements around the moving fronts. The implicit elements need to somehow follow the moving fronts as shown in Figure 5.2.
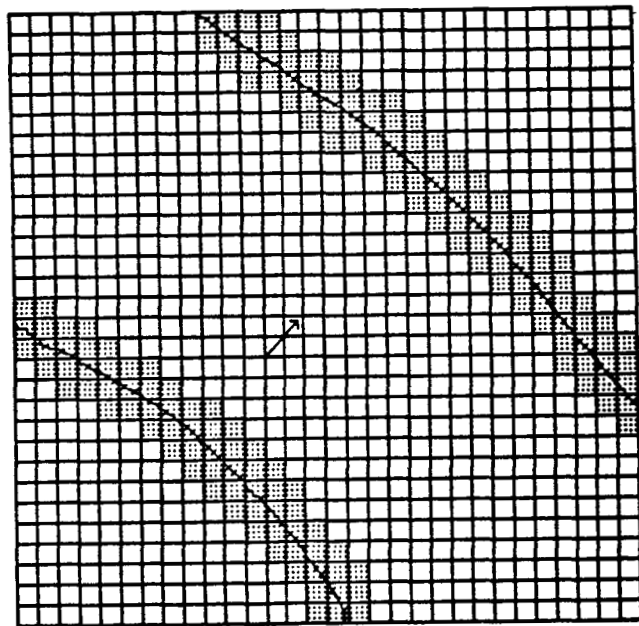
Fig. 5.2 Implicit element distribution in the moving front problem.

We propose that the sets $\mathcal{E}_I$ and $\mathcal{E}_E$ are determined dynamically. The determination will be based on several criteria including stability and accuracy considerations for all types of transport phenomena present. Stability and accuracy characteristics of algorithms are described not only in terms of the Courant numbers ($C_{\Delta t}$ and C_κ) but also in terms of the dimensionless wave number (see Figures 1(a)-3(f)). For the stability consideration, the elements for which the Courant numbers exceed the stability limit of the explicit schemes as described in Chapter 3 are assigned to be implicit while explicit elements are introduced elsewhere to save computer memory. The accuracy criterion is determined by the dimensionless wave number of the solution from the previous time step (or iteration). We can achieve this by defining a determination criterion which is based on some measure of the jump in the solution or jump in the flux across an element under consideration. The jump values are computed based on the previous time step (or iteration). Currently we employ the following definition for the jump in the solution across an element,

$$[\Phi] = \max_a (\Phi_a) - \min_a (\Phi_a), \qquad (5.12)$$

where "a" is the element node number. Note that the threshold value for this jump which makes the element eligible for the implicit set $\mathcal{E}_I$ should be based on the global scaling of the solution field. Such a global scaling idea is closely related to the global scaling concept of the "discontinuity capturing" scheme described in Tezduyar and Park [27].

In the adaptive implicit-explicit (AIE) approach, one can have a high degree of refinement throughout the mesh but can raise the implicit flag only for those elements which are proposed to be treated implicitly.

Compared to other adaptive concepts such as adaptive element redistribution or adaptive element-subdividing, the AIE scheme is far easier to implement because it involves no geometric changes; the bookkeeping involved is minimal.

Remark:

1. By appropriately numbering the nodes based on the distribution of the implicit elements. one can substantially reduce the bandwidth of the global matrices.

2. By the aid of bandwidth optimizer packages available in the market, one can renumber the nodes every time step (or every iteration) in the AIE calculations to efficiently save the computer memory.

CHAPTER 6

NUMERICAL EXAMPLES

The EBE, implicit-explicit, and AIE schemes have been tested on various problems governed by the model equations stated in Chapter 2. The results are compared with those obtained by the implicit and explicit schemes. The implicit solutions were shown by Ganjoo [28] and Glaisner [29] to be in agreement with the results from various past publications.

One-Dimensional Advection of a Cosine Wave

This problem consists of pure advection of a cosine wave from left to right. A cosine wave of unit amplitude is initially set in the left part of the domain. A uniform mesh containing 50 elements and 102 nodal points is employed. A homogeneous Dirichlet boundary condition is specified on the extreme left, and a homogeneous Neumann boundary condition is imposed on the extreme right. The advection velocity is 1.0 and the time step is such that the element Courant number is 0.6. Figures 6.1(a)-6.1(d) compare at the end of the same time interval the results obtained by various schemes. Figure 6.2 shows the distribution of impl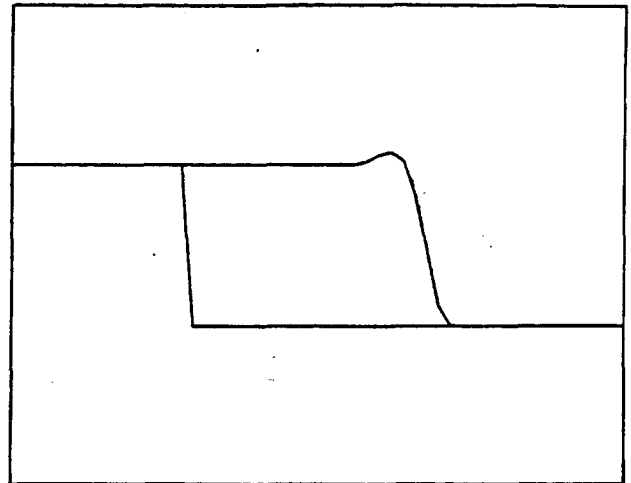icit elements for the AIE calculation at various time steps. The amplitude of the cosine wave decays to 0.969 for the implicit and EBE schemes, and to 0.965 for the adaptive implicit-explicit one-pass (AIE-1) scheme. A considerable decay of amplitude (to 0.769) is observed for the explicit one-pass (EXP-1) scheme.
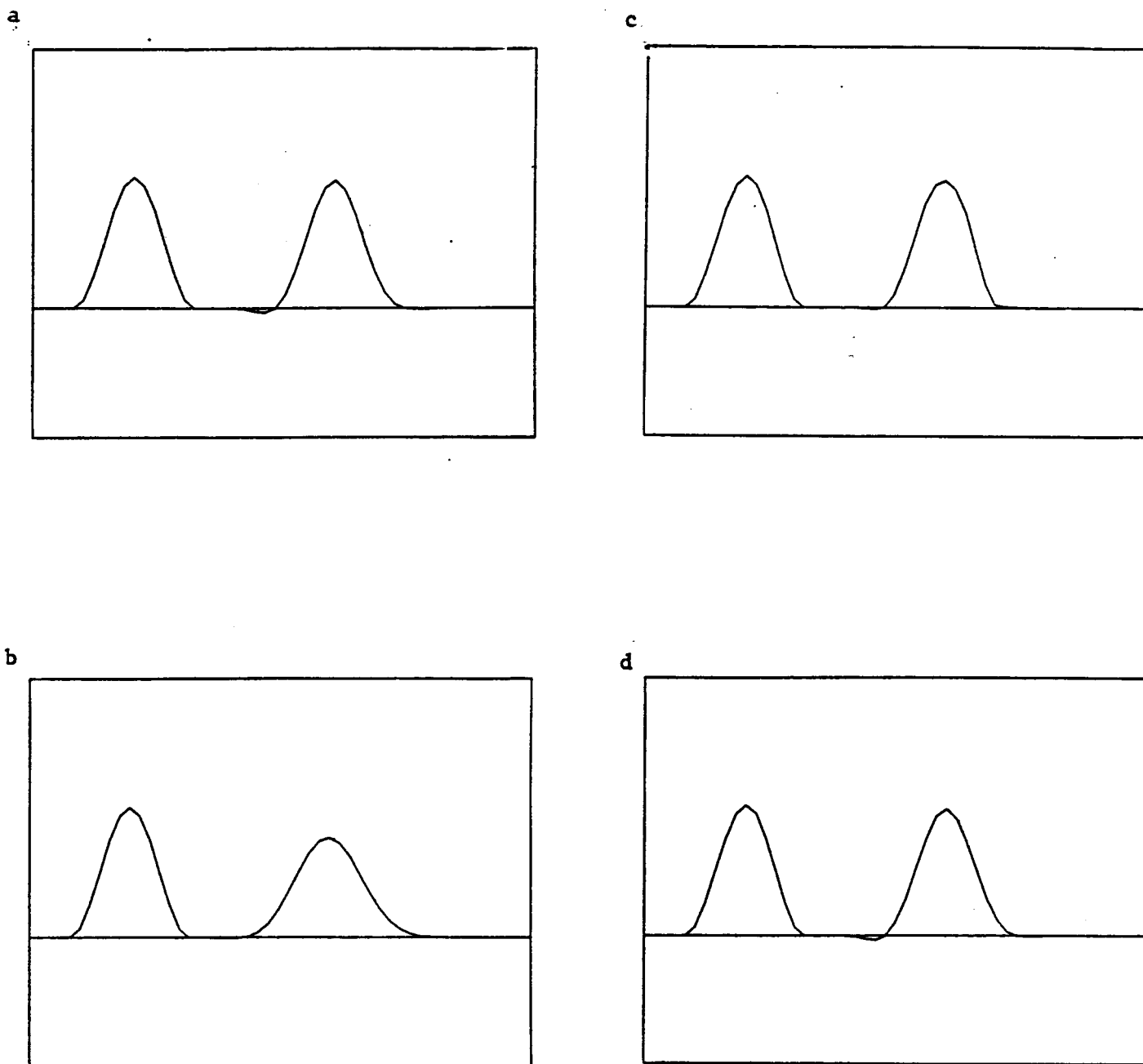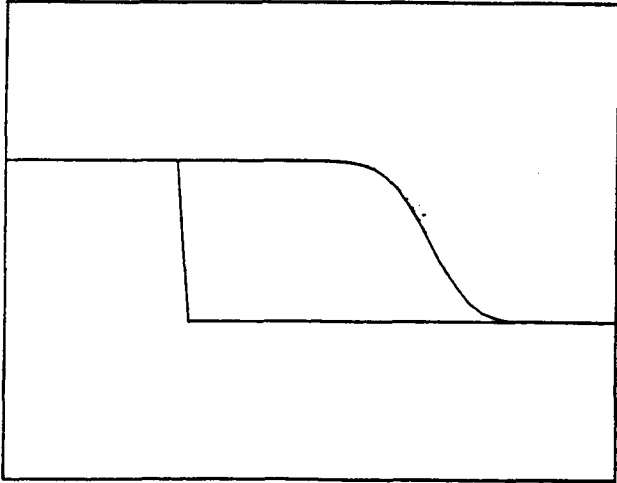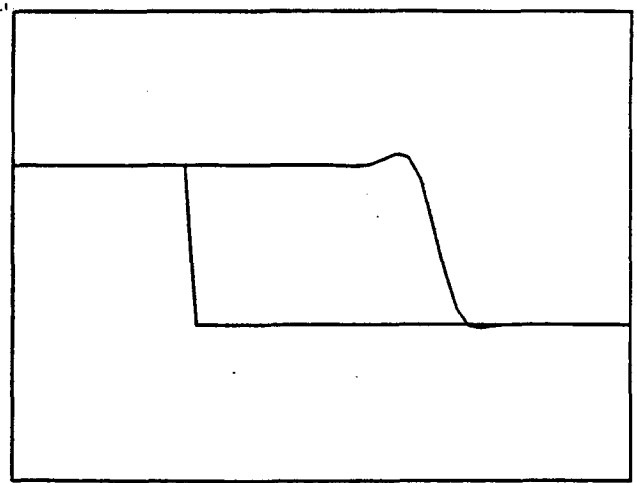
Fig. 6.1 One-dimensional advection of a cosine wave: Solution obtained by various schemes at t= 0.0 and 0.408 (a) Implicit scheme. (b) EXP-1. (c) AIE-1. (d) EBE.
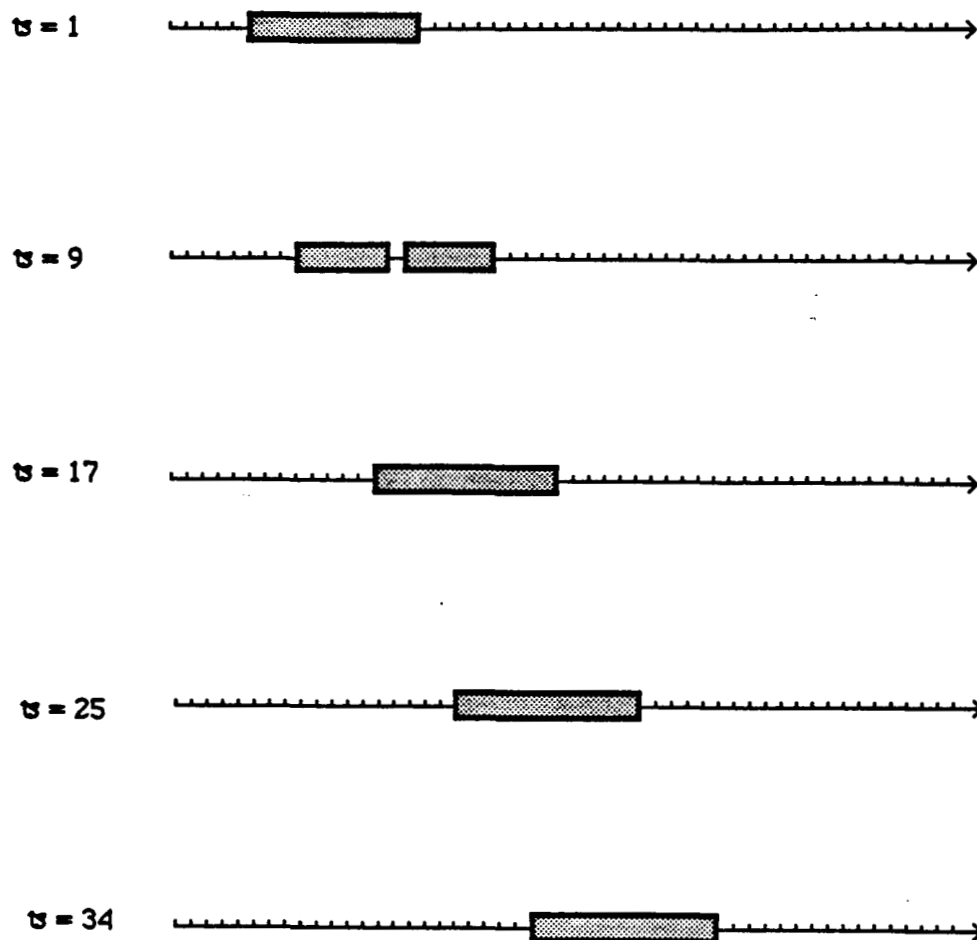
Fig. 6.2 One-dimensional advection of a cosine wave: Implicit elements in the AIE-1 calculation at various time steps.

One-Dimensional Advection of a Discontinuity

A discontinuity is advected from left to right under the same set-up conditions as the previous case. Figures 6.3(a)-6.3(d) show the results from various schemes at the end of the same time interval. Similar overshoots are found in the implicit, EBE, and AIE-1 schemes. Undershoot is observed in the implicit and EBE schemes. By changing the jump criterion described in Chapter 5, the same undershoot can be obtained in the AIE-1 scheme. The discontinuity becomes smeared in the EXP-1 scheme. Figure 6.4 shows the distribution of implicit elements for the AIE calculation at various time steps.

Two-Dimensional Advection of a Cosine Hill
(Translating Puff)

Two-dimensional advection and rigid body rotation of a cosine hill are typical examples for testing algorithms in convection-dominated problems (see, e.g., [30]). The translating puff problem consists of advection of a cosine hill from the extreme left to the right. Two meshes are tested: a uniform mesh with 30×30 elements in a 1×1 domain and a nonuniform mesh with 45×30 elements in a 1×0.75 domain. For the uniform mesh an initial cosine hill profile with unit peak amplitude and base radius of 0.2 is centered at $(x_1, x_2) = (0.267, 0.5)$. The diffusion coefficient is set to be 10^{-6}; the advection velocity is unity in x_1-direction, and the time step is adjusted to give a Courant number of 0.6. An homogeneous Dirichlet boundary condition is specified on all boundaries except at $x_1 = 1.0$ where an homogeneous Neumann boundary condition is imposed. Figures 6.5(a)-6.5(c) show the results at various times obtained by AIE-1. Figures 6.6(a) - 6.6(c) show the distribution of the implicit elements at the

a
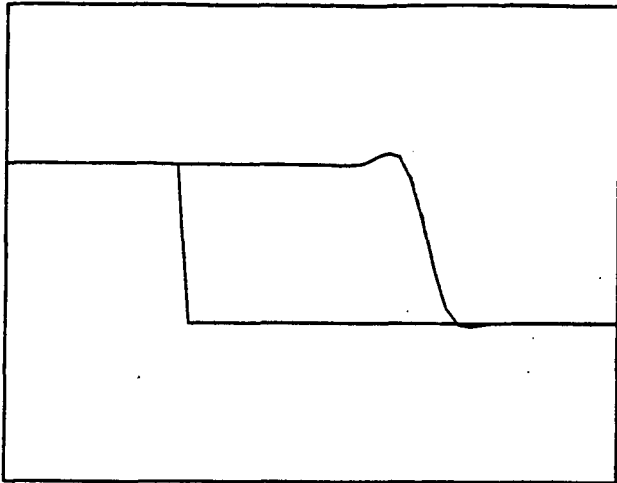
c

b

d

Fig. 6.3 One-dimensional advection of a discontinuity: Solution obtained by various schemes at t= 0.0 and 0.408 (a) Implicit scheme. (b) EXP-1. (c) AIE-1. (d) E B E.
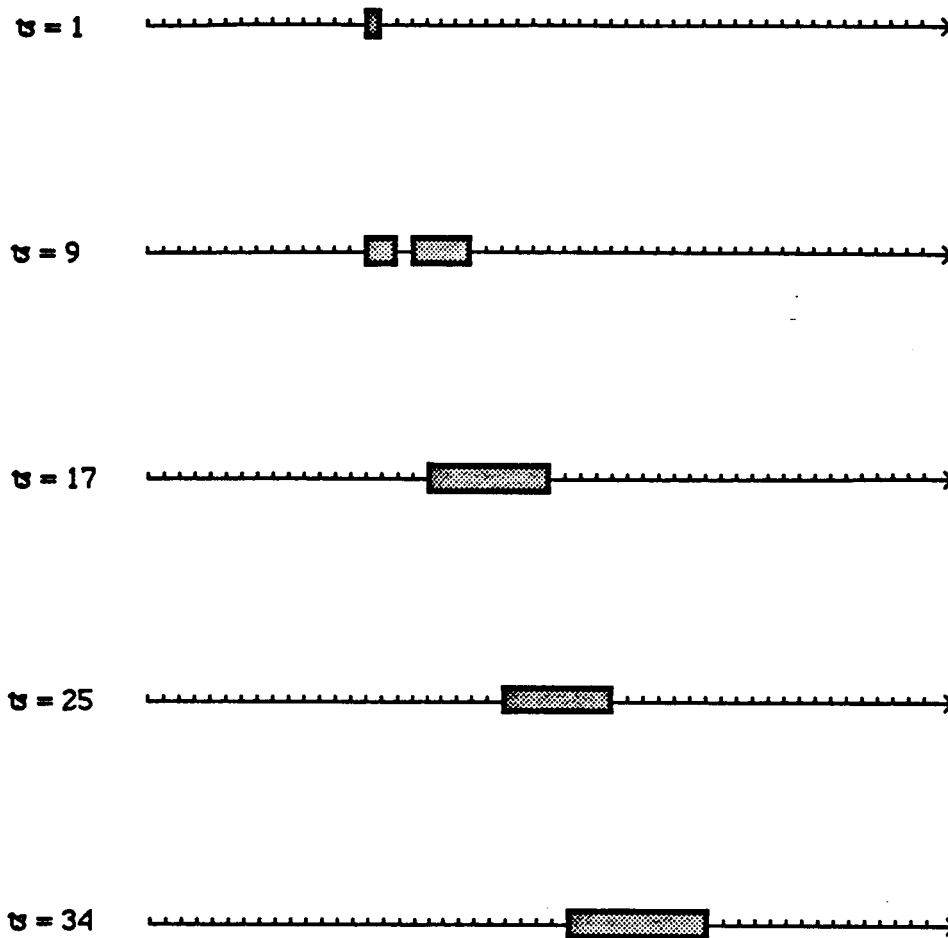
Fig. 6.4 One-dimensional advection of a discontinuity: Implicit elements in the AIE-1 calculation at various time steps.
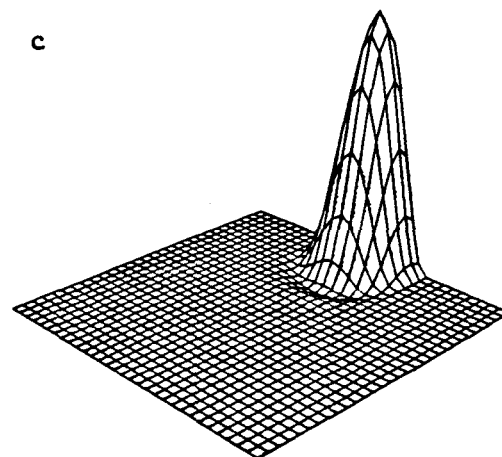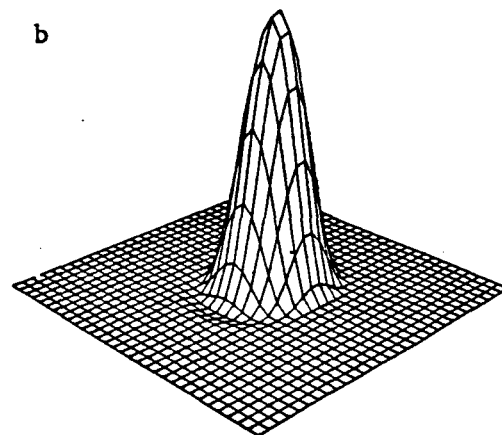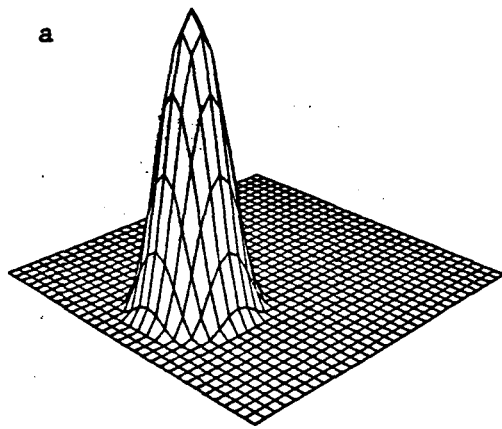
42

Fig. 6.5 Elevation plots for the translating
puff on a uniform mesh obtained by the
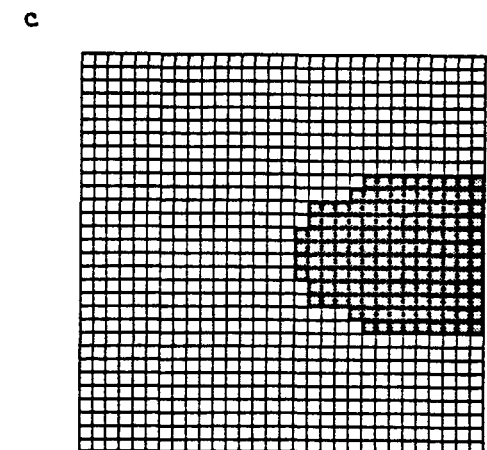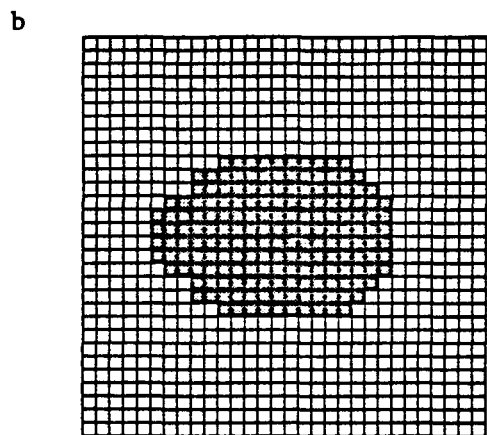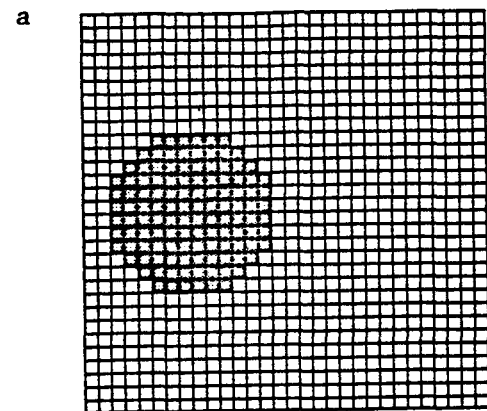AIE-1 scheme.(a) Initial condition.
(b) at t = 0.3. (c) at t = 0.72 .

Fig. 6.6 Distribution of the implicit
elements for the AIE-1 calculations
of the translating puff on a uniform
mesh. (a) at t = 0. (b) at t = 0.3.
(c) at t = 0.72.

43

corresponding times for the AIE-1 computations. Figures 6.7(a)-6.7(b) show the results at various time steps obtained by EXP-1. The peak amplitude value of the cosine hill at $t = 0.72$ is 0.972 for the implicit and EBE schemes and 0.974 for AIE-1. EXP-1 gives a stable solution with poor accuracy.

For the nonuniform mesh, the element length in the left region of the domain is half of that in the right region. The time step is chosen such that the Courant number is 1.8 in the left and 0.9 in the right. The initial profile is centered at $(x_1, x_2) =$ (0.233, 0.375) with base radius of 0.2. All other set-up conditions are the same as in the case of the uniform mesh. Figures 6.8(a)-6.8(c) show the elevation plots at various times obtained by the adaptive implicit-explicit two-pass scheme (AIE-2). Figures 6.9(a)-6.9(c) show the distribution of the implicit elements for the AIE-2 computations. The peak amplitude value at $t = 0.72$ is 0.969 for the implicit, EBE and AIE-2 schemes. The results for the explicit two pass (EXP-2) scheme are shown in Figures 6.10(a)-6.10(b). It can be seen in Figure 6.10(b) that in the left region of the domain the solution becomes unstable due to the high Courant number.

The mean bandwidth (averaged over the number of time steps) of the global coefficient matrix for the AIE scheme in the case of the uniform mesh is 25% of that for the implicit scheme. The average number of implicit elements at each time step is 173. For the nonuniform mesh the average mean bandwidth for the AIE scheme is 79%, and the average number of implicit elements is 1036.

Two-Dimensional Rigid Body Rotation of a Cosine Hill (Rotating Puff)

The set-up conditions for this problem are the same as in the uniform mesh case of the translating puff problem except that the velocity field is rotational with respect to
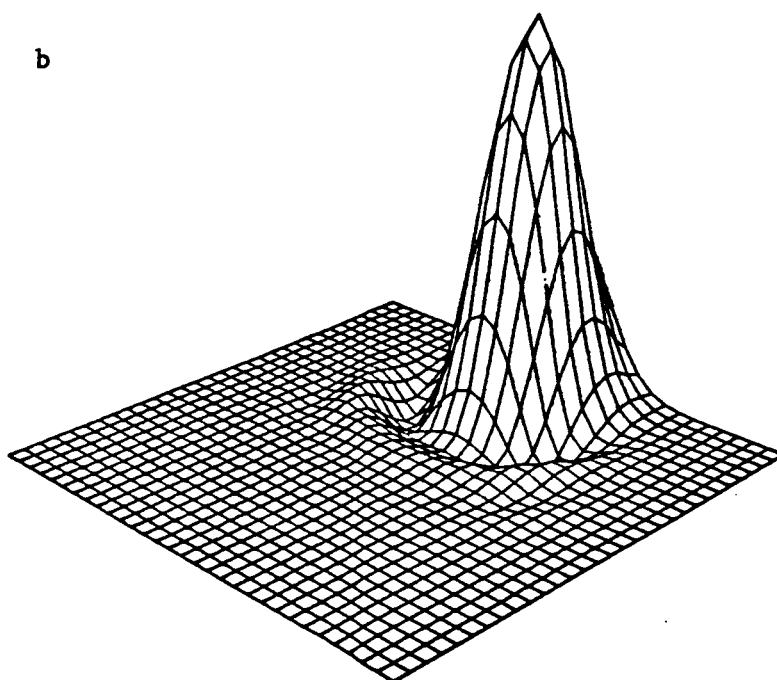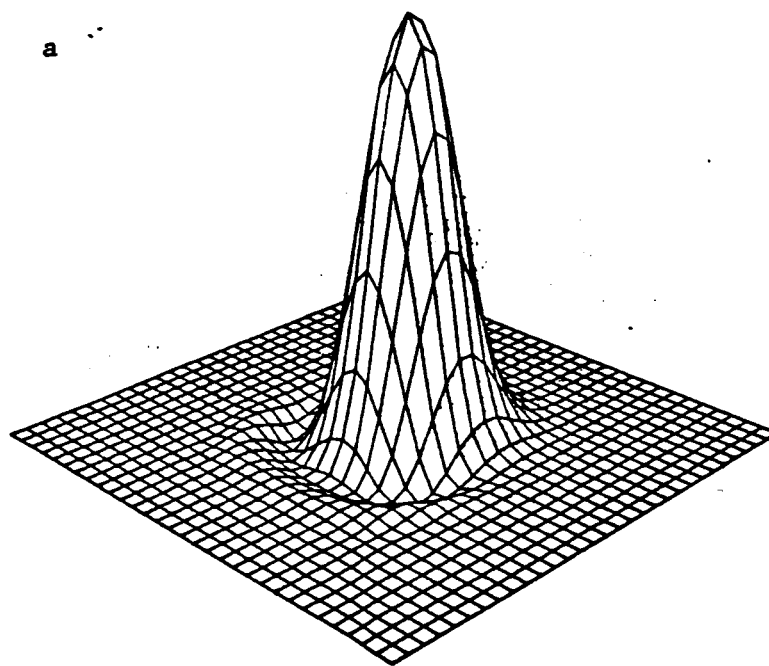
Fig. 6.7 Elevation plots for the translating puff on a uniform mesh obtained by the EXP-1 scheme. (a) at t = 0.3. (b) at t = 0.72.
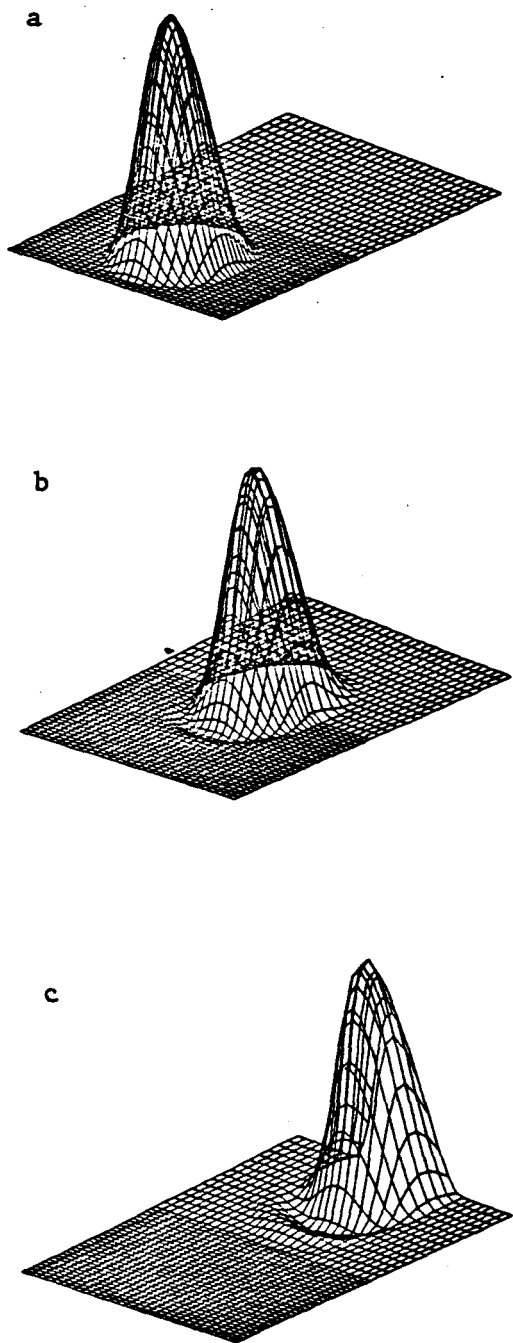
45

Fig. 6.8 Elevation plots for the translating puff on a nonuniform mesh obtained by the AIE-2 scheme. (a) Initial condition. (b) at t = 0.3. (c) at t = 0.72.

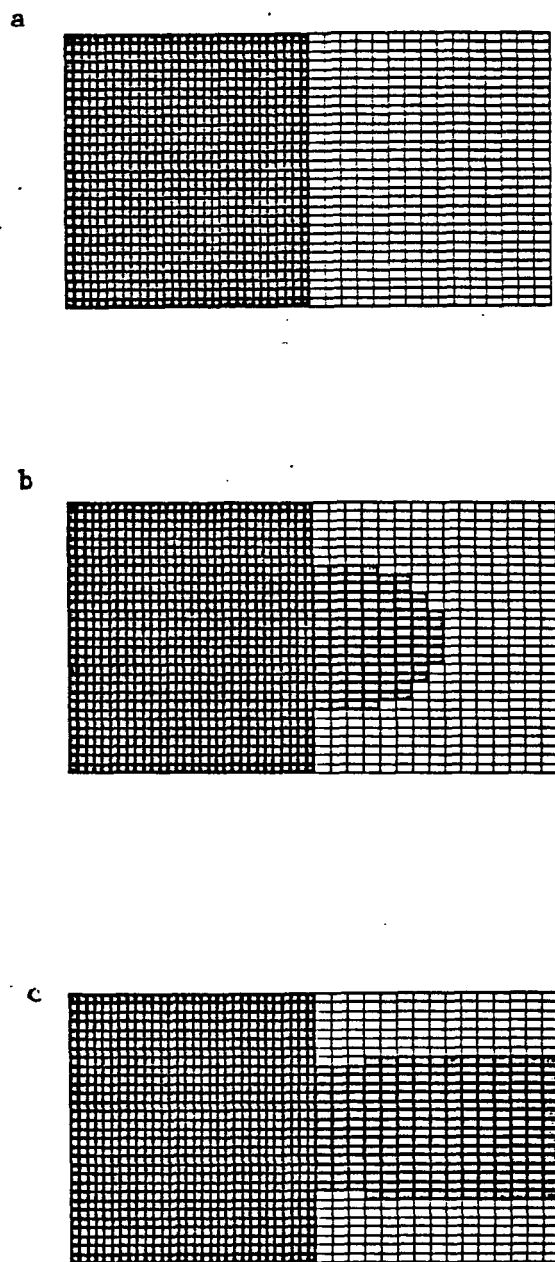Fig. 6.9 Distribution of the implicit elements for the AIE-2 calculations of the translating puff on a nonuniform mesh. (a) at t = 0.0. (b) at t= 0.3. (c) at t = 0.72.
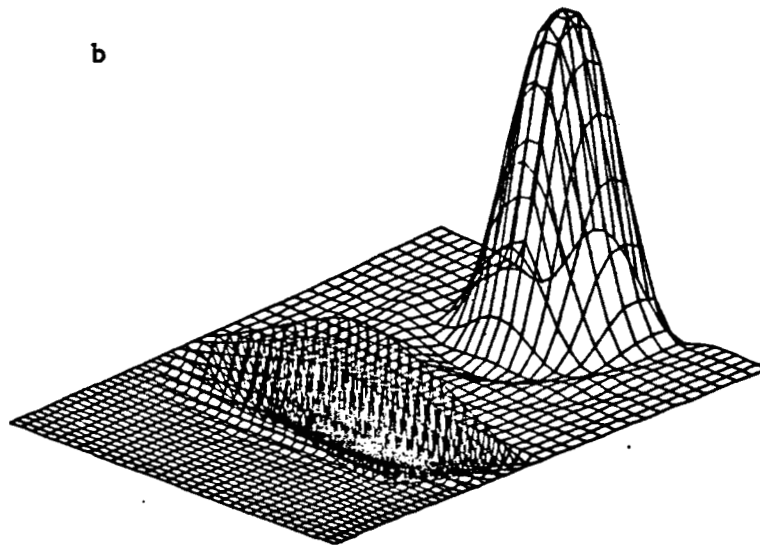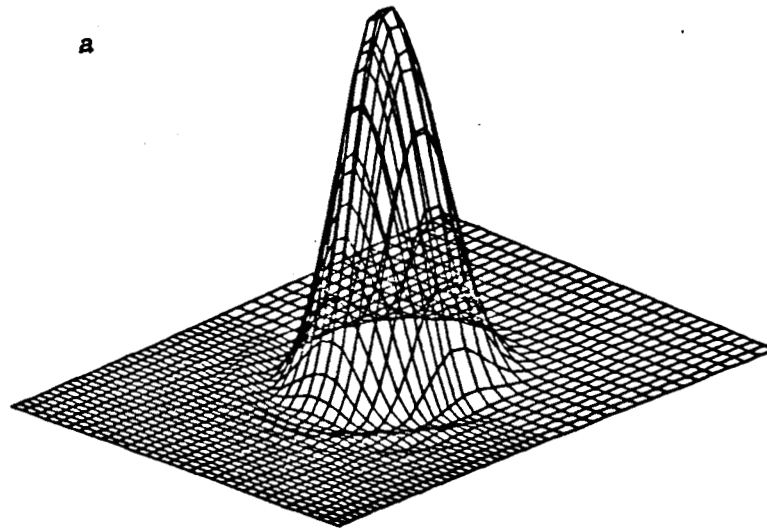
46

Fig. 6.10 Elevation plots for the translating puff on a nonuniform mesh obtained by the EXP-2 scheme. (a) at t = 0.3. (b) at t = 0.72.

the center of the domain (i.e., $u_1 = -x_2 + 0.5$, $u_2 = x_1 - 0.5$), and all boundary conditions are of the Dirichlet type and are homogeneous. The time step is adjusted to give a Courant number of 0.216 at the tip of the cosine hill. A full revolution is achieved in 200 time steps. Figures 6.11(a)-6.11(c) show the results at various times obtained by AIE-1. Figures 6.12(a)-6.12(c) show the distribution of the implicit elements at the corresponding times. The peak amplitude after a full revolution is found to be 0.984 for the implicit and EBE schemes, and 0.980 for AIE-1. The mean bandwidth (averaged over the number of time steps) for the AIE scheme is 26% of the implicit scheme. The average number of implicit elements at each time step is 173. As in the case of the translating puff (uniform mesh), the results for EXP-1 are not satisfactory. Figures 6.13(a)-6.13(b) demonstrate the performance of EXP-1 in this problem.

Shock Structure/ Entropy Condition Test Problem

The problem is governed by equation (2.11). A computational domain of unit length is taken. The number of elements is 40. The initial condition is shown in frame 0 of Figure 6.14. The explicit solution is very close to the implicit solution such that there is no need to test the AIE scheme in this problem. EBE and the implicit schemes are compared. The differences are indistinguishable. The results obtained by the EBE scheme are shown in Figure 6.14. Each frame corresponds to a time step of $\Delta t = 0.6$. As can be observed, the initial condition contains two stable shocks and one unstable shock. The unstable shock immediately breaks down, and eventually the two stable shocks merge to form a steady shock. Figure 6.15 shows the history of the EBE iterations (number of pseudo-time iterations in the first corrector step versus the
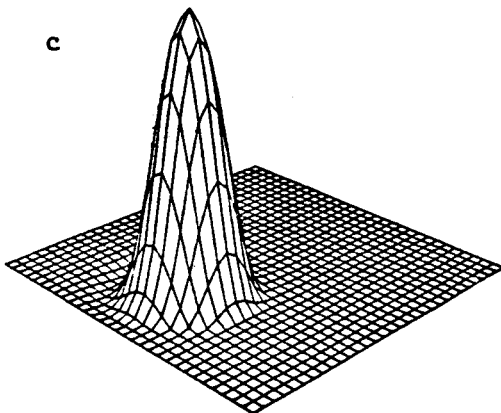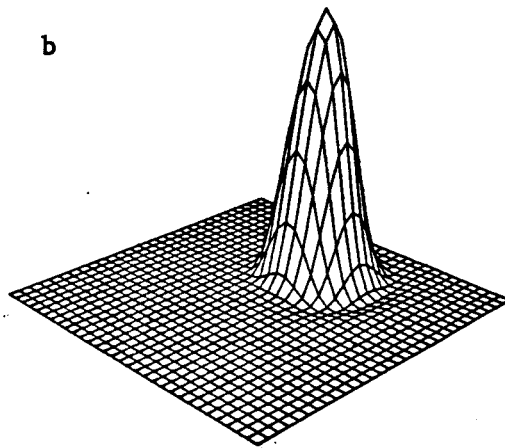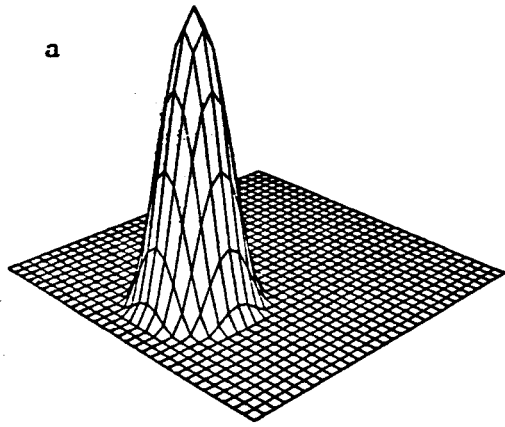
48

Fig. 6.11 Elevation plots for the rotating
puff obtained by the AIE-1 scheme.
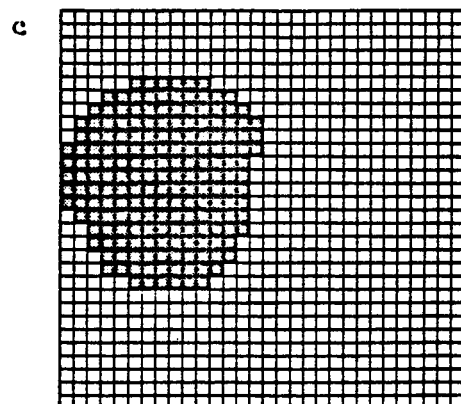(a) Initial condition. (b) at t = 3.14 .
(c) at t = 6.28.
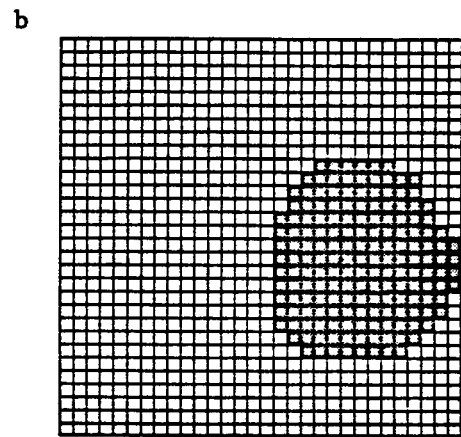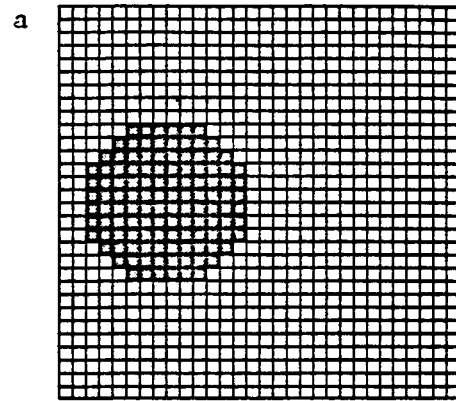
Fig. 6.12 Distribution of the implicit
elements for the AIE-1 calculations of the
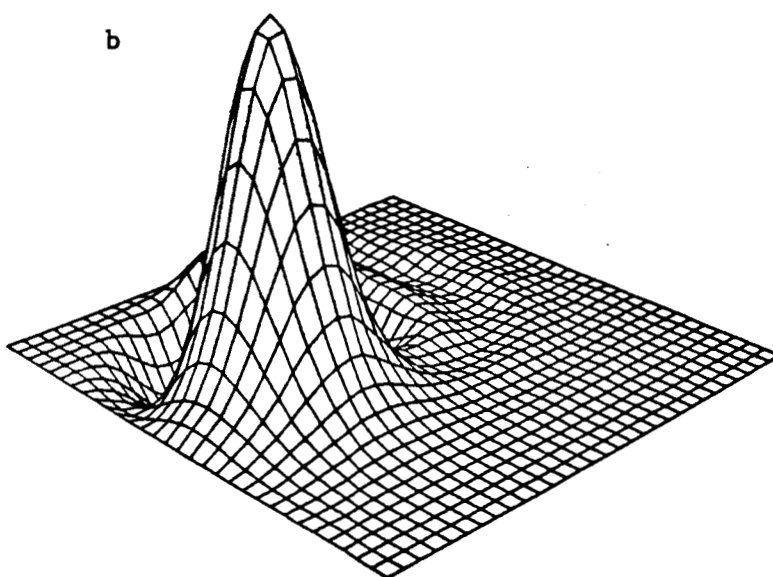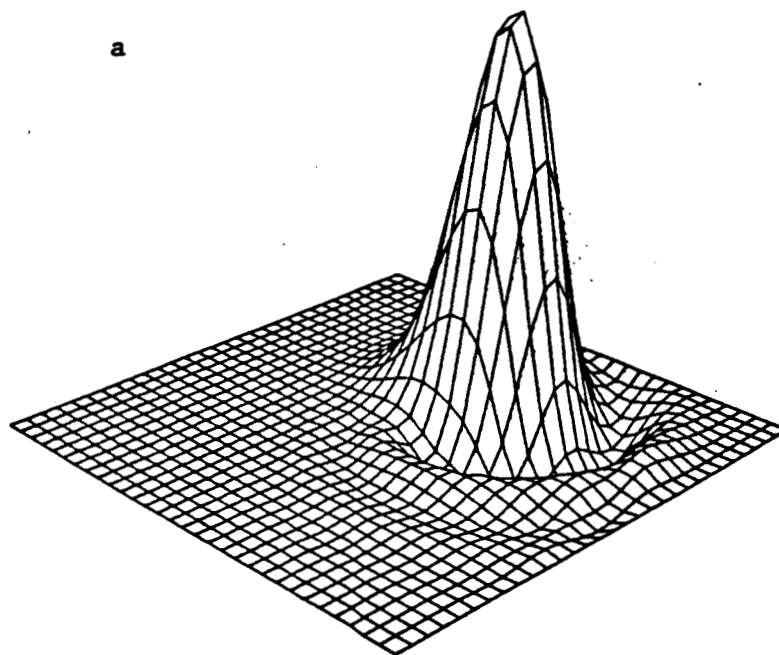rotating puff. (a) at t = 0 . (b) at t = 3.14.
(c) at t = 6.28 .

Fig. 6.13 Elevation plots for the rotating puff obtained by the EXP-1 scheme.
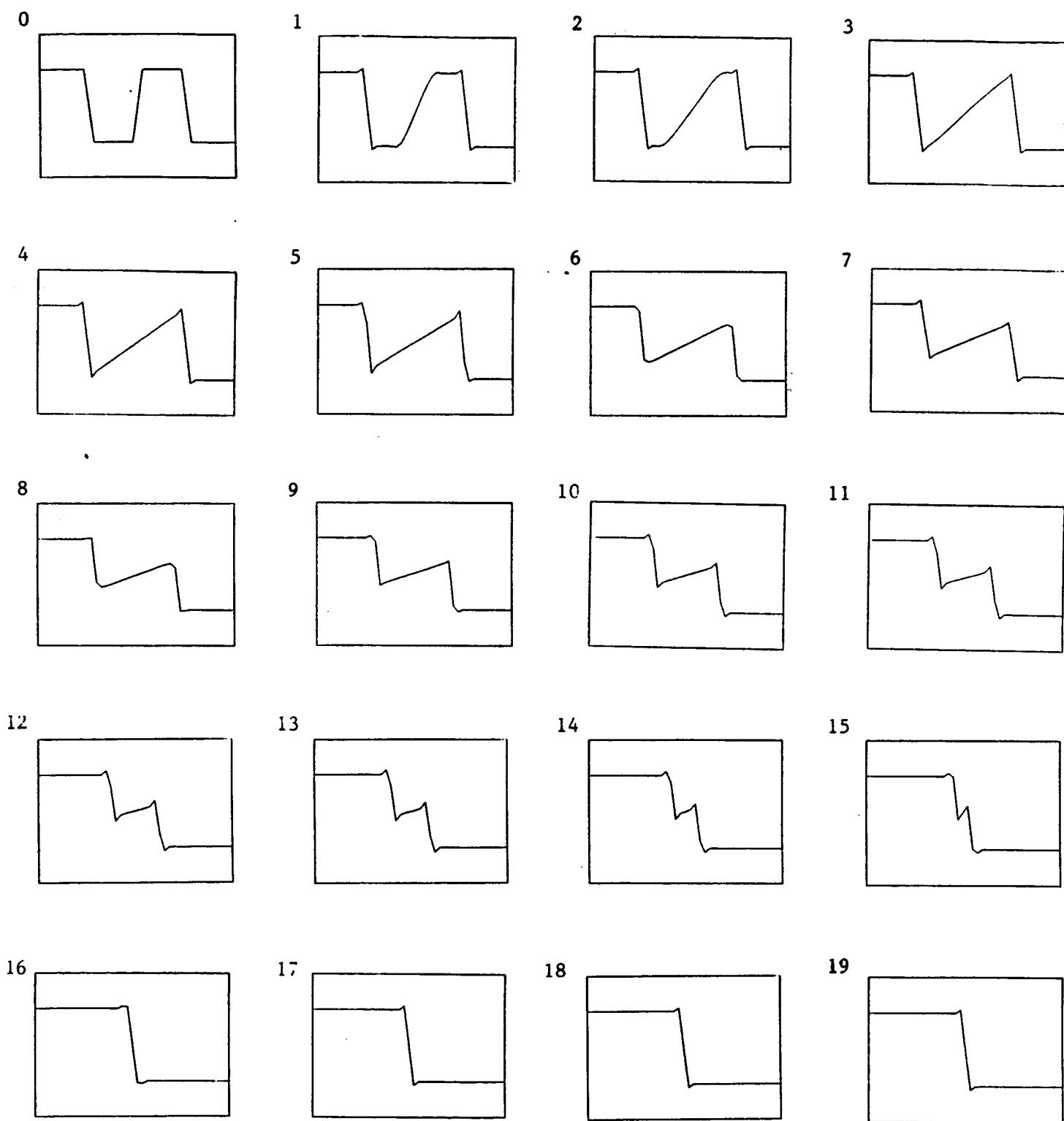(a) at t = 3.14. (b) at t = 6.28.

Fig. 6.14 Shock structure/entropy condition test problem: Solutions obtained by the EBE scheme at various time steps.

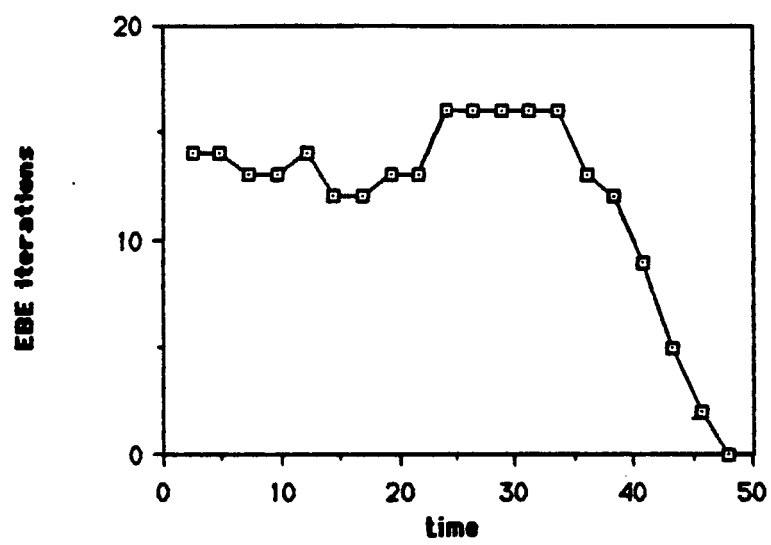Fig. 6.15 Shock structure /entropy condition test problem: History of the number of EBE iterations.

corresponding time).

Flow Past a Circular Cylinder

A two-dimensional viscous flow past a circular cylinder has been of special interests among researchers in the field of computational fluid dynamics (see, e.g., [31,32]). In this problem we have 1940 elements and 2037 nodal points. A refined and implicit zone is located around the cylinder. Diffusivity is 0.0025 giving a Reynolds number of 100 based on the diameter of the cylinder. The time step is fixed at 1.0. The number of corrections at each time step is allowed to be as many as the convergence criterion (10^{-6}) dictates.The mesh, the boundary conditions, and the distribution of the implicit elements are shown in Figure 6.16. Figures 6.17(a)-6.17(c) show the streamlines, relative streamlines and isovorticity lines for the symmetric solution at time = 700 obtained by the implicit-explicit (IMEX) scheme. After that, an artificial disturbance is placed shortly to initiate a nonsymmetric solution. Figures 6.18(a)-6.18(c) show the nonsymmetric results at time = 1,200 obtained by the EBE scheme. The implicit and the implicit-explicit schemes all give very close results (differences less than 0.5%). The explicit scheme diverges. The mean bandwidth of the implicit-explicit scheme is 47% of the implicit scheme. The number of implicit elements is 320.
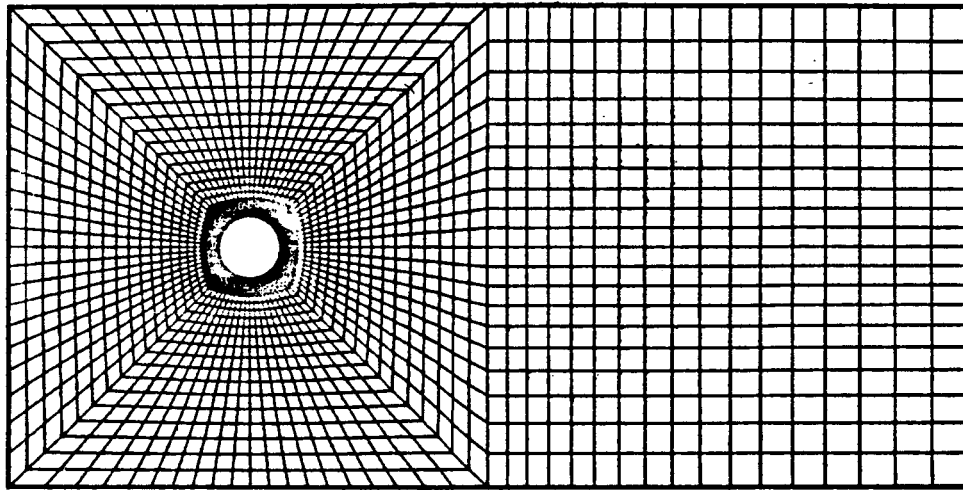
Driven Cavity Flow

Because of the discontinuity of the velocity at the corners, driven-cavity flow problem has become an important example for testing a numerical method during the recent years (see, e.g., [33]). In this problem, the flow velocity is zero on three

$\Psi = 1$, $\omega = 0$

$\Psi = 0.125 \times y$,

$\omega = 0$.

$\partial\Psi/\partial n = 0$,

$\partial\omega/\partial n = 0$.

$\Psi = -1$, $\omega = 0$

* $\Psi = 0$, $\partial\Psi/\partial n = 0$ on the cylinder.

Fig. 6.16 Flow past a circular cylinder at Reynolds number 100: Finite element mesh, boundary conditions and the distribution of the implicit elements for the IMEX calculations.

a
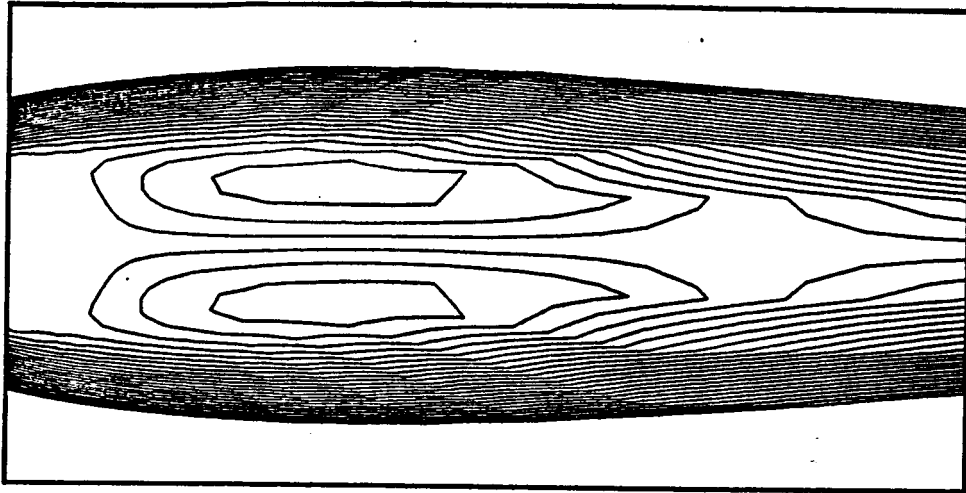
b
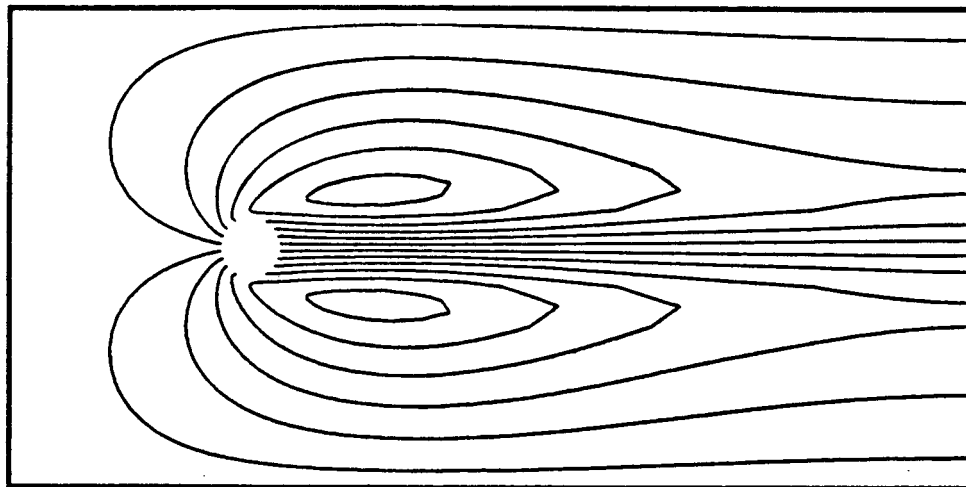
c

Fig. 6.17 Flow past a circular cylinder at Reynolds number 100: Symmetric solutions obtained by the EBE scheme at t = 700 (a) Local streamlines. (b) Relative streamlines. (c) Isovorticity lines.
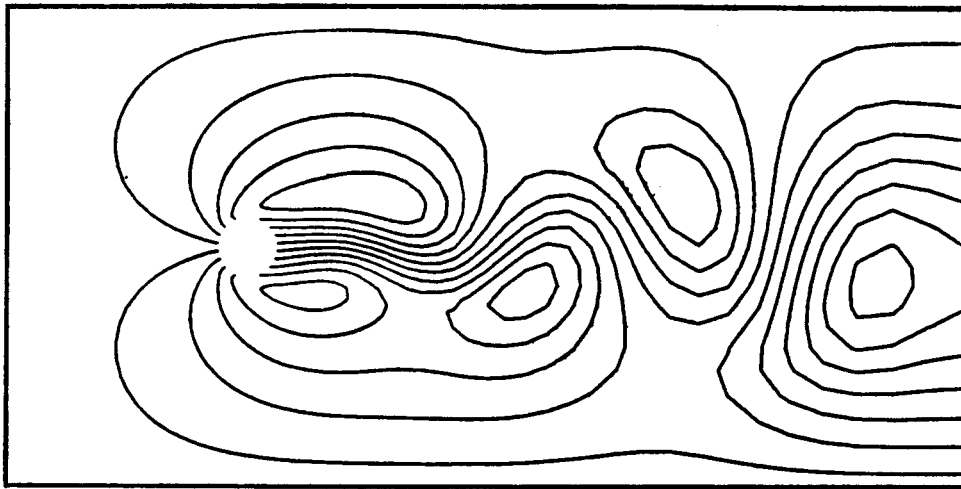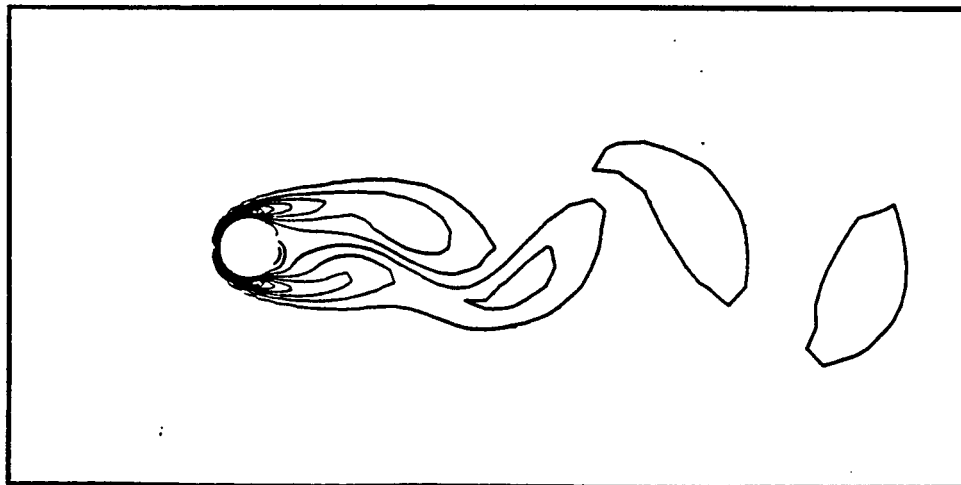
Fig. 6.18. Flow past a circular cylinder at Reynolds number 100. Nonsymmetric solutions obtained by the EBE scheme at t = 1200. (a) Local streamlines. (b) Relative streamlines. (c) Iso vorticity lines.

sides and unity on the fourth side. A uniform mesh of 30×30 elements in a 1×1 domain is chosen. Diffusivity is 0.0025, time step is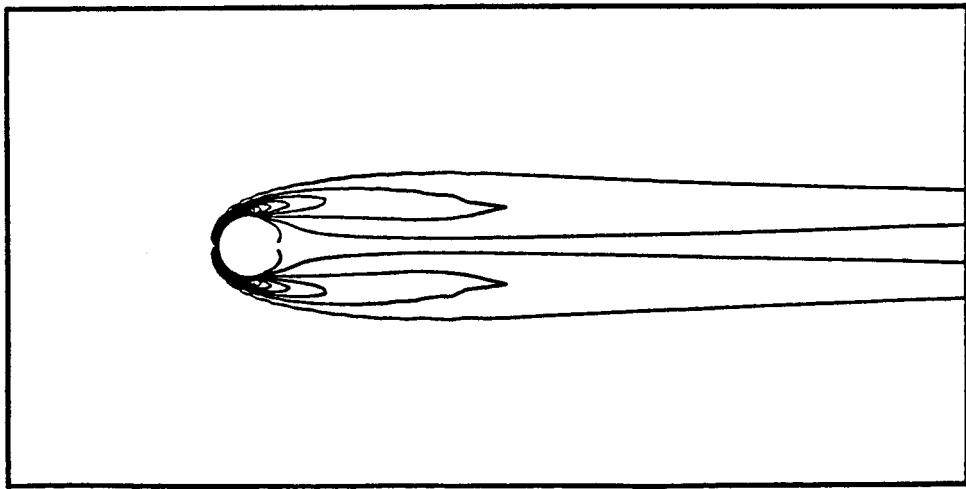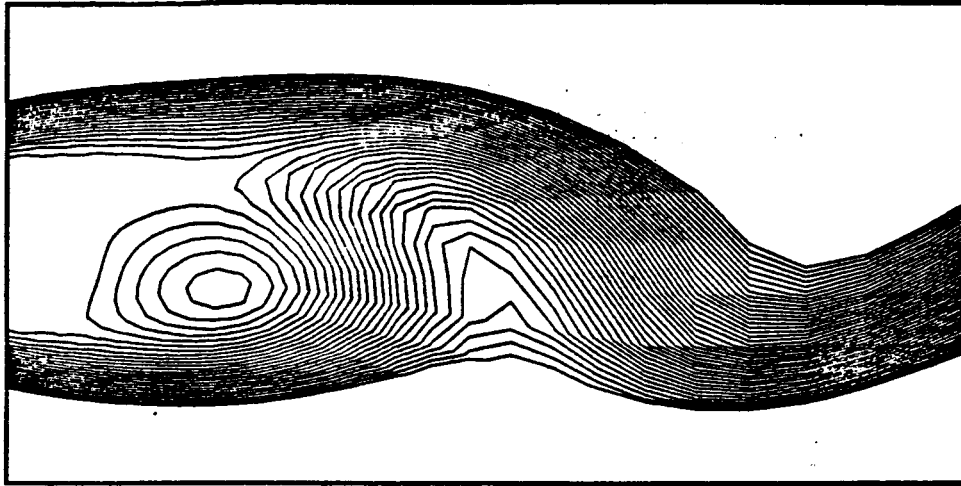 0.1, and Reynolds number is 400 based on the side length of the square domain. The number of corrections at each time step is limited to 5. Figure 6.19(a) shows the mesh, the boundary conditions, and the distribution of the implicit elements. Results obtained by the IMEX scheme are shown in Figures 6.19(b)-6.19(d). Those results are indistinguishable from the implicit and EBE solutions (differences less than 0.001%) . The mean bandwidth for implicit-explicit scheme is 44% of the implicit scheme. The number of implicit elements is 403.

a

$\Psi = 0$, $\partial\Psi/\partial n = 1.$

$\Psi = 0$,
$\partial\Psi/\partial n = 0.$

$\Psi = 0$,
$\partial\Psi/\partial n = 0.$

$\Psi = 0$, $\partial\Psi/\partial n = 0.$

c

b

d

Fig. 6.19. Driven-cavity flow at Reynolds number 400: Solutions obtained by the IMEX scheme at t = 10. (a) Finite Element mesh, boundary conditions and the distribution of the implicit elements. (b) Streamlines. (c) Corner streamlines. (d) Isovorticity lines.

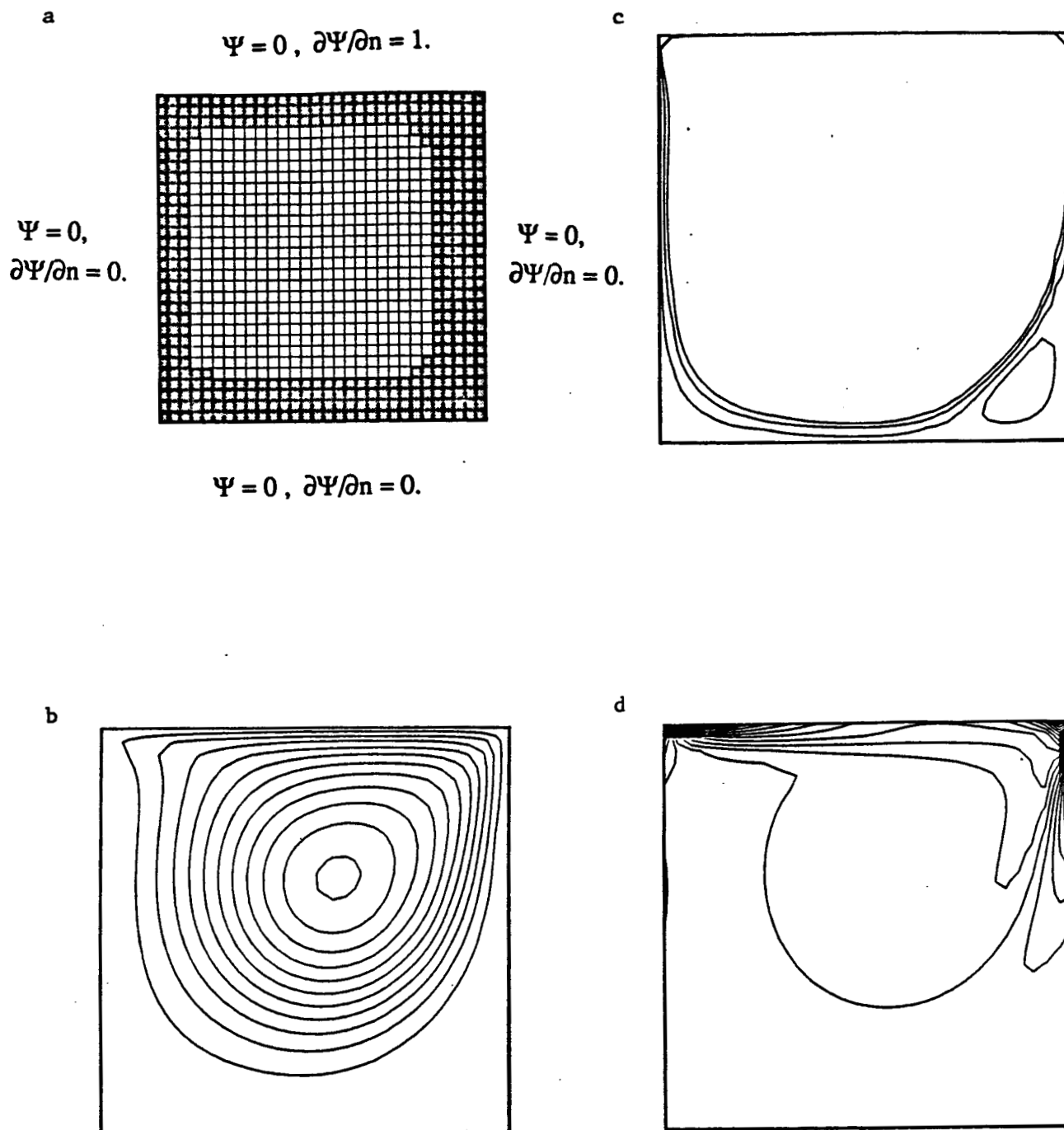CHAPTER 7

CONCLUSIONS

In this report, we have presented approximate solution schemes for large
equation systems resulting from finite-element formulation of fluid dynamics
problems. The element-by-element (EBE) approximate factorization scheme is
essentially an iterative scheme which totally eliminates the need for the formation,
storage, and inversion of a large global matrix. All computations are performed at the
element level. The method keeps the versatility of the finite-element formulation in its
easy adjustment to irregular mesh and its easy implementation to boundary conditions
and source terms. Futhermore, the EBE approximate factorization procedure is
parallelizable and this aspect of it makes it especially favorable since parallel
computations are expected to play a more and more important role in computational
fluid dynamics.

Implicit-explicit schemes in nature are approximations to implicit schemes, yet
they substantially reduce the cost of formation, storage, and inversion of a large global
matrix. In this approach, for the elements which are designated to be implicit, the
element level matrices are kept as they are, whereas for the explicit elements the
element level matrices are approximated by a diagonal matrix. In the adaptive
implicit-explicit (AIE) scheme, the implicit elements are selected adaptively. Selection
of the implicit and explicit elements is based on several criteria including the stability
and accuracy. For the stability consideration, the elements for which the Courant
number exceed the stability limit of the explicit scheme are assigned to be implicit,

while explicit elements are introduced elsewhere to reduce cost in computer memory. The accuracy criterion is determined by the dimensionless wave number of the solution from the previous time step (or iteration). By appropriately numbering the nodes based on the distribution of the implicit elements, one can substantially reduce the bandwidth of global matrices. This scheme allows us to have implicit refinement where it is needed. Compared to other adaptive concepts such as element redistribution or element subdividing, the AIE scheme is far easier to implement.

We have applied these schemes to various problems governed by the convection-diffusion equation and the vorticity stream-function form of the two-dimensional Navier-Stokes equations. Streamline-Upwind/ Petrov-Galerkin formulations are employed for the spatial discretization of our model problems and a predictor-corrector algorithm is used to solve the resulting semi-discrete equation system. The results obtained by EBE, IMEX and AIE in all cases are indistinguishable from those obtained by the true implicit formulations while the storage required is substantially reduced. The savings in the storage of the coefficient matrix in various test problems are summarized in Table 7.1. Recently the author has developed a new finite-element procedure for vorticity stream-function formulation in which the coefficient matrix derived from the Poisson's equation is symmetric and positive-definite [34]. For procedures which involve symmetric positive-definite matrices, convergence of the EBE, IMEX and AIE schemes are more predictable.

The results indicate a great potential for the future work in this area. It is believed that it will not be very long before these schemes are accepted as powerful tools in large-scale computing.

Case	Savings in the storage of the coefficient matrix	Scheme
Translating Puff (uniform mesh)	75 %	AIE-1
Translating Puff (nonuniform mesh)	21 %	AIE-2
Rotating Puff	74 %	AIE-1
Flow past a Circular Cylinder	53 %	IMEX
Driven Cavity Flow	56 %	IMEX

Table 7.1 Savings in the storage of the coefficient matrix for various test problems.

* no renumbering of the nodes (see Remark (2) in Chapter 5)

REFERENCES

[1] R. Glowinski, Q. V. Dinh, and J. Periaux," Domain Decomposition Methods for Nonlinear Problems in Fluid Dynamics," Computer Methods in Applied Mechanics and Engineering, 40 (1983), pp. 27-109.

[2] C. C. Paige and M. A. Saunders," LSQR: An Algorithm for Sparse Linear Equations and Sparse Least Square," ACM Transactions on Mathematical Software, 8 (1982), pp. 43-71.

[3] G. W. Stewart," Conjugate Direction Methods for Solving Systems of Linear Equations," Numer. Math., 21 (1973), pp. 285-297.

[4] D. M. Young," Second-Degree Iterative Methods for the Solution of Large Linear Systems," J. Approx. Theory, 5 (1972), pp. 137-148.

[5] R. S. Rogallo," Numerical Experiments in Homogeneous Turbulence," NASA TN 81315, September 1981.

[6] D. Heller," A Survey of Parallel Algorithms in Numerical Linear Algebra," SIAM Review, 20 (1978), pp. 740-777.

[7] J. M. Frailong and J. Pakleza," Resolution of General Partial Differential Equations on a Fixed Size SIMD/MIMD Large Celluar Processor," in

Proceedings of the IMACS International Congress, Sorente, Italie, (Sept. 1979).

[8] R. Glowinski," Numerical Methods for Nonlinear Variational Problems," Springer-Verlag, New York, 1984.

[9] D. W. Peaceman and H. H. Rachford," The Numerical Solution of Parabolic and Elliptic Differential Equations," J. Soc. Indust. Appl. Math. 3 (1955), pp. 28-41.

[10] J. Douglas, H. H. Rachford," On the Numerical Solution of Heat Conduction Problems in Two and Three Space Variables," Trans. Am. Math. Soc. , 82 (1956), pp. 421-439.

[11] N.N. Yanenko," The Method of Fractional Steps," Springer-Verlag, New York, 1971.

[12] T. J. R. Hughes, I. Levit and J. Winget," Element-By-Element Implicit Algorithms for Heat Conduction," Journal of the Engineering Mechanics Division, ASCE, 109 (1983), pp. 576-585.

[13] T. J. R. Hughes, I. Levit and J. Winget," An Element-by-Element Solution Algorithm for Problems of Structural and Solid Mechanics," Computer Methods in Applied Mechanics and Engineering, 36 (1983), pp. 241-254.

[14] T. J. R. Hughes, J. Winget, I. Levit, T. E. Tezduyar," New Alternating

Direction Procedures in Finite Element Analysis Based upon EBE Approximate Factorizations," Computer Methods for Nonlinear Solids and Mechanics, S. N. Atluri and N. Perrone, eds., AMD Vol. 54 (1983), ASME, New York, pp.75-110.

[15] T. J. R. Hughes and W. K. Liu, " Implicit-Explicit Finite Elements in Transient Analysis: Stability Theory," Journal of Applied Mechanics, 45 (1978), pp. 371-374.

[16] T.J.R. Hughes and W.K. Liu," Implicit-Explicit Finite Elements in Transient Analysis: Implementation and Numerical Examples," Journal of Applied Mechanics, 45 (1978), pp. 375-378.

[17] G. F. Carey and J. T. Oden," Finite Elements: Computational Aspects," Volume III, Prentice-Hall Inc., Englewood Cliffs, 1983, pp. 23-125.

[18] M.O. Bristeau, R. Glowinski, and J. Periaux," Numerical Methods for the Navier-Stokes Equations Applications to the Simulation of Compressible and Incompressible Viscous Flows," Research Report UH/MD-4, February 1987, pp. 50-69.

[19] T. E. Tezduyar, R. Glowinski, and F. Glaisner," Streamline-Upwind/Petrov Galerkin Procedures for the Vorticity-Stream Function Form of the Navier-Stokes Equations," presented in the 5th International Conference on Numerical Methods in Laminar and Turbulent Flow, to be published.

[20] R. Wait," Function Spaces," The Mathematical Basis of Finite Element Methods, D. F. Griffiths, ed., Oxford University Press, New York, 1984, pp.1-13.

[21] T.E. Tezduyar and D.K. Ganjoo," Petrov-Galerkin Formulations with Weighting Functions Dependent upon Spatial and Temporal Discretization: Applications to Transient Convection-Diffusion Problems," Computer Methods in Applied Mechanics and Engineering, 59 (1986), pp. 47-71.

[22] A.N. Brooks and T.J.R. Hughes," Streamline Upwind/Petrov-Galerkin Formulations for Convection Dominated Flows with Partial Emphasis on the Incompressible Navier-Stokes Equations," Computer Methods in Applied Mechanics and Engineering, 32 (1982), pp.199-259.

[23] T. J. R. Hughes," Analysis of Transient Algorithms with Particular Reference to Stability Behavior," Computational Methods for Transient Analysis, Ted Belytschko and T.J.R. Hughes, eds., North Holland Publishing Co., Amsterdam, 1984, pp. 67-153.

[24] W. H. Raymond and A. K. Parrot," Generalized Galerkin Methods for First Order Hyperbolic Equations," Journal of Computational Physics, 12(1973), pp. 435-461.

[25] T. E. Tezduyar and T. J. R. Hughes," Development of Time-accurate Finite Element Techniques for First-order Hyperbolic System with Particular Emphasis

on the Compressible Euler Equations," Final Report, NASA-Ames University Consortium Interchange No. NCA2-OR745-104, April 1982.

[26] G. F. Carey and J. T. Oden," Finite Elements: Computational Aspects," Volume III, Prentice-Hall Inc., Englewood Cliffs, 1983, pp. 253-318.

[27] T. E. Tezduyar and Y. J. Park," Discontinuity-Capturing Finite Element Formulations for Nonlinear Convection-Diffusion-Reaction Equations," Computer Methods in Applied Mechanics and Engineering, 59 (1986), pp.307-325.

[28] D. K. Ganjoo," Petrov-Galerkin Formulations for Various Transport Problems," M.S. Thesis, University of Houston, Department of Mechanical Engineering, 1986.

[29] F. Glaisner, " Finite Element Techniques for the Navier-Stokes Equations in the Primitive Variables Formulation and the Vorticity Stream-Function Formulation," M.S. Thesis, University of Houston, Department of Mechanical Engineering, 1987.

[30] P. M. Gresho and R. L. Lee," Don't Suppress the Wiggles-They Are Telling You Something !," Finite Element Methods for Convection Dominated Flows, T. J. R. Hughes, ed., AMD Vol. 34 (1979) , ASME, New York.

[31] B. Fornberg," A Numerical Study of Steady Viscous Flow Past a Circular

Cylinder," J. Fluid Mech., 98 (1980), pp.819-855.

[32] M. Braza, P. Chassaing and H. HaMinh," Numerical Study and Physical Analysis of the Pressure and Velocity Fields in the Near Wake of a Circular Cylinder," J. Fluid Mech., 165 (1986), pp. 79-130.

[33] R. Peyret and T. D. Taylor," Computational Methods for Fluid Flow," Springer-Verlag, New York, 1983, pp. 199-207.

[34] M.O. Bristeau, R. Glowinski, and J. Periaux," Numerical Methods for the Navier-Stokes Equations Applications to the Simulation of Compressible and Incompressible Viscous Flows," Research Report UH/MD-4, February 1987, pp. 50-69.